LOAN DOCUMENT

PHOTOGRAPH THIS SHEET

AD-A233 569

DTIC ACCESSION NUMBER

LEVEL

1

INVENTORY

WL-TR-91-3033 Vol III

DOCUMENT IDENTIFICATION

APR 1991

DISTRIBUTION STATEMENT A
Approved for public release;
Distribution Unlimited

DISTRIBUTION STATEMENT

ACCESSION FOR
NTIS GRA&I ☒
DTIC TRAC ☐
UNANNOUNCED ☐
JUSTIFICATION

BY
DISTRIBUTION/
AVAILABILITY CODES

DISTRIBUTION	AVAILABILITY AND/OR SPECIAL	
A-1		

DISTRIBUTION STAMP

DTIC
ELECTE
APR 16 1991
S E D

DATE ACCESSIONED

HANDLE WITH CARE

DATE RETURNED

DATE RECEIVED IN DTIC

REGISTERED OR CERTIFIED NUMBER

PHOTOGRAPH THIS SHEET AND RETURN TO DTIC-FDAC

WL-TR-91-3033
Volume III

AD-A233 569

CALCULATION OF HIGH ANGLE OF ATTACK AERODYNAMICS OF FIGHTER CONFIGURATIONS; VOLUME III- UNSTEADY

C. Edward Lan, H. Emdad, Suei Chin
P. Sundaram, S. C. Mehrotra, and
R. K. Tripathi

Vigyan Research Associates, Inc.
30 Research Dr
Hampton VA 23666-1325

April 1991

Final Report for Period Aug 87 - Jan 90

Approved for public release; distribution is unlimited.

FLIGHT DYNAMICS DIRECTORATE
WRIGHT LABORATORY
AIR FORCE SYSTEMS COMMAND
WRIGHT-PATTERSON AIR FORCE BASE, OHIO 45433-6553

NOTICE

When Government drawings, specifications, or other data are used for any purpose other than in connection with a definitely Government-related procurement, the United States Government incurs no responsibility or any obligation whatsoever. The fact that the government may have formulated or in any way supplied the said drawings, specifications, or other data, is not to be regarded by implication, or otherwise in any manner construed, as licensing the holder, or any other person or corporation; or as conveying any rights or permission to manufacture, use, or sell any patented invention that may in any way be related thereto.

This report is releasable to the National Technical Information Service (NTIS). At NTIS, it will be available to the general public, including foreign nations.

This technical report has been reviewed and is approved for publication.

Charles B. Heath

CHARLES B. HEATH
DesignPredictions Group

FOR THE COMMANDER

James E. Hunter

JAMES E. HUNTER
Flight Control Division

If your address has changed, if you wish to be removed from our mailing list, or if the addressee is no longer employed by your organization please notify WL/FIGC, WPAFB, OH 45433-6553 to help us maintain a current mailing list.

Copies of this report should not be returned unless return is required by security considerations, contractual obligations, or notice on a specific document.

UNCLASSIFIED
SECURITY CLASSIFICATION OF THIS PAGE

REPORT DOCUMENTATION PAGE

Form Approved OMB No. 0704-0188

1a REPORT SECURITY CLASSIFICATION: Unclassified

1b RESTRICTIVE MARKINGS: None

2a SECURITY CLASSIFICATION AUTHORITY:

2b DECLASSIFICATION / DOWNGRADING SCHEDULE:

3 DISTRIBUTION / AVAILABILITY OF REPORT: Approved for Public Release: Distribution is Unlimited

4 PERFORMING ORGANIZATION REPORT NUMBER(S):

5 MONITORING ORGANIZATION REPORT NUMBER(S): WL-TR-91-3033 Volume III

6a NAME OF PERFORMING ORGANIZATION: Vigyan Research Associates, Inc

6b OFFICE SYMBOL *(If applicable)*:

7a NAME OF MONITORING ORGANIZATION: Flight Dynamics Directorate (WL/FIGC) Wright Laboratory

6c ADDRESS *(City, State, and ZIP Code)*: 30 Research Dr, Hampton VA 23666-1325

7b ADDRESS *(City, State, and ZIP Code)*: WPAFB OH 45433-6553

8a NAME OF FUNDING / SPONSORING ORGANIZATION:

8b OFFICE SYMBOL *(If applicable)*:

9 PROCUREMENT INSTRUMENT IDENTIFICATION NUMBER: F33615-87-C-3616

8c ADDRESS *(City, State, and ZIP Code)*:

10 SOURCE OF FUNDING NUMBERS

PROGRAM ELEMENT NO	PROJECT NO	TASK NO	WORK UNIT ACCESSION NO
65502F	3005	40	09

11 TITLE *(Include Security Classification)*: Calculation of High Angle of Attack Aerodynamics of Fighter Configurations, Volume III - Unsteady

12 PERSONAL AUTHOR(S): C. E. Lan, H. Emdad, S. Chin, P. Sundaram, S. C. Mehrotra, and R. K. Tripathy

13a TYPE OF REPORT: Final

13b TIME COVERED: FROM Aug 87 TO Jan 90

14 DATE OF REPORT *(Year, Month, Day)*: April 1991

15 PAGE COUNT: 59

16 SUPPLEMENTARY NOTATION: This is a Small Business Innovative Research Program, Phase II report.

17 COSATI CODES

FIELD	GROUP	SUB-GROUP

18 SUBJECT TERMS *(Continue on reverse if necessary and identify by block number)*: Stability and Control; High Angle of Attack Aerodynamics

19 ABSTRACT *(Continue on reverse if necessary and identify by block number)*

A computational method for unsteady aerodynamics of fighter configurations at high angles of attack is developed. The leading-edge vortices are represented by free vortex filaments which are adjusted iteratively to satisfy the force-free condition. The small-disturbance, unsteady potential equation is solved in the frequency domain for motions in pitching, plunging, flapping, side movement, rolling, and yawing oscillation in compressible flow. Computed results in rolling moment coefficients due to side acceleration are compared with data for 60-deg and 80-deg delta wings. Lateral-directional characteristics for an F-106b configuration are also compared with data obtained in forced-oscillations tests. It is shown that reasonable results can be obtained by the present unsteady flow method, but not by steady flow theory. Calculation of dynamic stall effects on a rectangular wing of aspect ratio 4 is demonstrated by using experimental section data. Although no data for the wing are available, the results appear plausible. Industrial usage of this has produced mixed results. At this time, the use of these methods in a production manner is recommended.

20 DISTRIBUTION / AVAILABILITY OF ABSTRACT: ☒ UNCLASSIFIED/UNLIMITED ☐ SAME AS RPT ☐ DTIC USERS

21 ABSTRACT SECURITY CLASSIFICATION: Unclassified

22a NAME OF RESPONSIBLE INDIVIDUAL: Charles B. Heath

22b TELEPHONE *(Include Area Code)*: (513) 255-8480

22c OFFICE SYMBOL: WL/FIGC

DD Form 1473, JUN 86 — *Previous editions are obsolete* — SECURITY CLASSIFICATION OF THIS PAGE

UNCLASSIFIED

LIST OF SYMBOLS

Symbol	Definition	Usual Dimension
b	(Wing) span	ft
c	Chord	ft
c_{ℓ}	Section lift coefficient	
C_L	Lift coefficient	
C_y	Side force coefficient	
C_{ℓ}	Rolling moment coefficient	
C_{ℓ_p}	$= \partial C_{\ell}/\partial(pb/2V_\infty)$	
$C_{\ell_{\dot\beta}}$	$= \partial C_{\ell}/\partial(\dot\beta b/2V_\infty)$	
C_{ℓ_r}	$= \partial C_{\ell}/\partial(rb/2V_\infty)$	
$C_{n_{\dot\beta}}$	$= \partial C_n/\partial(\dot\beta b/2V_\infty)$	
C_N	Normal force coefficient	
C_n	Yawing moment coefficient	
$C_{n_{\dot\beta}}$	$= \partial C_n/\partial(\dot\beta b/2V_\infty)$	
C_p	Pressure coefficient	
ΔC_p	Lifting pressure coefficient	
d	Sideway displacement	ft
h	Plunging amplitude	ft
$k = \frac{\omega \ell_r}{V}$	Reduced frequency	
ℓ_r	Reference length	ft
M	Mach number	
N_c	Number of chordwise discrete elements	
N_s	Number of spanwise strips	
$\hat{n}$	Unit normal vector	

TABLE OF CONTENTS

SUMMARY

A computational method for unsteady aerodynamics of fighter configurations at high angles of attack is developed. The leading-edge vortices are represented by free vortex filaments which are adjusted iteratively to satisfy the force-free condition. The small-disturbance, unsteady potential equation is solved in frequency domain for motions in pitching, plunging, flapping, side movement, rolling, and yawing oscillation in compressible flow. Computed results in rolling moment coefficients due to side acceleration are compared with data for 60-deg and 80-deg delta wings. Lateral-directional characteristics for an F-106 B configuration are also compared with data obtained in forced-oscillation test. It is shown that reasonable results can be obtained by the present unsteady-flow method, but not by the steady-flow theory. Calculation of dynamic stall effect on a rectangular wing of aspect ratio 4 is demonstrated by using experimental sectional data. Although no data for the wing are available for comparison, the results appear to be plausible.

LIST OF SYMBOLS, continued

Symbol	Definition	Usual Dimension
P	Roll rate	rad/sec
p	Pressure	lb/ft^2
Δp	Pressure differential	lb/ft^2
q	Pitch rate	rad/sec
r	Yaw rate	Rad/sec
r_1	$= \sqrt{y_o^2 + z_o^2}$	
R	$= \sqrt{x_o^2 + \beta^2(y_o^2 + z_o^2)}$	ft
Re	Real part	
S	Area	ft^2
u	Backwash	ft/sec
U	x-component of velocity	ft/sec
V	Freestream velocity	ft/sec
v	y-component of velocity	ft/sec
w	z-component of velocity	ft/sec
x, y, z	Rectangular coordinates	ft
x_a	X coordinate of pitching axis	ft
x_o	$= x - \xi$	
y_o	$= y - \eta$	
z_c	Camber ordinate	ft
z_o	$= z - \zeta$	

LIST OF SYMBOLS, continued

Symbol	Definition	Usual Dimension
Greek Symbols		
α	Angle of attack	rad
α_e	Effective angle of attack	rad
α_s	Steady angle of attack	rad
$\Delta\alpha$	Incremental angle of attack	rad
β	$\sqrt{1 - M^2}$	
β	Sideslip angle	rad
ω	Oscillation frequency	rad/sec
ϕ	Velocity potential	ft^2/sec
$\bar{\phi}_r$	Unsteady roll angle	rad
θ	Pitching amplitude or integration variable	rad
ξ, η, ζ	Rectangular coordinates of elemental doublet	ft
γ	Circulation density	ft/sec
Γ	Circulation	ft^2/sec
ψ	Yawing angle	
τ	Dihedral angle	
$\dot{\beta}$	Rate of sideslip angle	rad/sec
$\dot{r}$	Yawing acceleration	rad/sec^2
$\dot{p}$	Rolling acceleration	rad/sec^2

LIST OF SYMBOLS, continued

Symbol	Definition	Usual Dimension
Subscript		
1	Unsteady	
eff	Effective	
ℓ	Leading edge	
s	Steady	
t	Trailing edge	
u	Unsteady	
∞	Freestream	

1. INTRODUCTION

When a fighter aircraft performs maneuvers at high angles of attack, the aerodynamic forces and moments acting on the aircraft are, in general, dependent nonlinearly, not only on the motion variables but also on the time rate of change of these motion variables. To predict the dependency on motion variables, such as the dihedral effect (C_{ℓ_β}), the VORSTAB-II code was developed (ref. 1). The code is based on a steady-flow theory, so that the unsteady aerodynamic effect on stability parameters cannot be accounted for. This shortcoming is particularly serious in predicting dynamic stability parameters, such as roll-damping derivatives, at high angles of attack (ref. 1). This is because in an unsteady rolling motion about the body axis, dynamic change in sideslip will be induced to result in rolling moment coefficient due to side acceleration (i.e. $C_{\ell_{\dot\beta}}$). The latter may provide additional damping or undamping, depending on configurations. In fact, significant effect of $C_{\ell_{\dot\beta}}$ on flight dynamics has already been illustrated in the past (refs. 2 and 3). These dynamic stability parameters can only be calculated through the unsteady aerodynamic theory.

In general, the unsteady aerodynamic theory, relative to a steady-flow theory, provides the following mechanisms to affect the dynamic stability parameters:

- aerodynamic lag in attached flow;
- vortex lag in vortex flow, including dynamic vortex-breakdown effect;

- dynamic boundary layer and stall effect in viscous flow.

The aerodynamic lag in attached flow is produced by convective effect of shed vortices and the finite speed of disturbance propagation in a compressible flow. This effect is automatically included in any appropriate inviscid unsteady aerodynamic theory in compressible flow.

On the other hand, vortex lag effect is important when a wing with edge-separated vortex flow is in an unsteady motion. This effect has been modeled in the past through the method of suction analogy in compressible flow (ref. 4), the method of separated vortex filaments in incompressible flow (refs. 5-7), and the solution of Navier-Stokes equations. The method of references 5-7 has been illustrated only for simple wing planforms in incompressible flow and is based on a time-step integration for the solution. The solution of Navier-Stokes equations for airplane configurations is too "computation intensive" for applications to preliminary design.

Several empirical modeling methods for dynamic stall effect on airfoil sections have been proposed as summarized in reference 8. Accuracy of Navier-Stokes solutions in two- and three-dimensional flows is uncertain, in particular in deep dynamic stall regime.

In this investigation, the effect of vortex lag is modeled by using unsteady discrete vortex filaments in compressible flow. This is done by converting the VORSTAB-II code into an unsteady version in frequency domain. The main objective is to calculate dynamic

stability parameters. For the dynamic stall effect on a wing, a method based on using 2-D test data is proposed.

2. THEORETICAL APPROACH

2.1 General Concept

The basic methodology considered in the present investigation is based on the subsonic unsteady potential equation with correct· .ns for steady boundary layer separation and embedded oscillatory free vortex filaments for vortex flow effects. The unsteady potential flow calculation is based on the small disturbance equation. Only harmonic motions will be considered. By the assumption of small amplitudes of motion, the solution can be expressed as the sum of two components, one representing steady flow and the other being oscillatory. It is assumed that the solution for some sinusoidal motion of a wing with frequency ω can be expressed in the form of

$$\phi(x, y, z, t) = \phi_s(x, y, z) + \phi_1(x, y, z)e^{i\omega t} \tag{1}$$

where ϕ is the velocity potential, and ϕ_s is the steady-state solution, which is a function of the spatial coordinates x, y, and z. ϕ_1 is an unsteady component and is a complex function, thus allowing for phase differences between the motion and the resulting flow field.

In the present method the lifting surface is represented by a distribution of oscillatory horseshoe vortex, which is the exact solution of the unsteady small disturbance equation. The strength of the vortex can be obtained by satisfying the boundary condition on the lifting surfaces. To properly account for the leading-edge

singularity of pressure loading in the linear theory, and hence the leading-edge thrust, the unsteady Quasi-Vortex-Lattice Method (UQVLM) is used (ref. 4).

In addition, the oscillatory vortex flow arising from separation along the leading and side edges of a low aspect ratio wing is simulated by using discrete free oscillatory vortex filaments. The mathematical expression for the latter will be derived later.

Note that unsteady fuselage effect is not investigated in this study.

2.2 Unsteady Potential Flow Theory

The unsteady small disturbance potential equation in a moving coordinate system is

$$\left(1 - \frac{U^2}{a_\infty^2}\right) \frac{\partial^2\phi}{\partial x^2} + \frac{\partial^2\phi}{\partial y^2} + \frac{\partial^2\phi}{\partial z^2} \frac{1}{a_\infty^2} \frac{\partial^2\phi}{\partial t^2} - \frac{2U}{a_\infty^2} \frac{\partial^2\phi}{\partial x \partial t} = 0 \tag{2}$$

By the application of the method found in reference 4, the above equation can be reduced into the following integral equation:

$$\phi(x,y,z,t) = \frac{1}{4\pi} \iint_S \left[\frac{\partial}{\partial \zeta} \int_{\frac{MR - x_o}{1 - M^2}}^{\infty} \frac{1}{\rho_\infty U_\infty} \Delta p\left(\xi,\eta,t - \frac{\tau + x_o}{U_\infty}\right)\left(\frac{1}{r}\right)\partial\tau\right](\partial\xi\partial\eta) \tag{3}$$

where

$$r = \sqrt{\tau^2 + y_o^2 + z_o^2}$$

ϕ is actually the solution of equation (2) and represents a doublet or oscillatory horseshoe vortex with the strength of ΔC_p. By

introducing the harmonic time variation such that for any t_o

$$\Delta p(\xi, \eta, t_o) = \mathrm{Re}[\Delta\bar{p}(\xi, \eta)e^{i\omega t_o}]$$

$$\phi(\xi, \eta, t_o) = \mathrm{Re}[\bar{\phi}(x, y, z)e^{i\omega t_o}] \tag{4}$$

After substitution of (4) into (3):

$$\bar{\phi}(x, Y, z) = \frac{1}{4\pi} \iint_S \frac{\Delta\bar{p}(\xi, \eta)}{\rho_\infty U_\infty} \kappa(x_o, y, z, K, M)d\xi d\eta \tag{5}$$

where κ is defined as

$$\kappa = \frac{\partial}{\partial\zeta} \int_{\frac{-x_o+MR}{1-M^2}}^{\infty} e^{-\frac{i\omega}{U_\infty}(\tau+x_o)} \frac{1}{r}\, d\tau$$

Since equation (3) is equivalent to a doublet, the solution of equation (2) can be represented by doublet distributions. The thin wing approximation is used throughout.

To calculate the induced velocity, due to a unit strength of doublet at any (x, y, z) location, the method of reference 4 will be followed. The resulting equations are

$$w = \frac{\partial\phi}{\partial z} = \sum \int_{x_\ell}^{x_t} \Delta C_{p_u}(\xi)\left(\frac{\partial\phi_1}{\partial z} + \frac{\partial\phi_2}{\partial z}\right)d\xi$$

$$v = \frac{\partial\phi}{dy} = \sum \int_{x_\ell}^{x_t} \Delta C_{p_u}(\xi)\left(\frac{\partial\phi_1}{\partial y} + \frac{\partial\phi_2}{\partial y}\right)d\xi$$

$$u = \frac{\partial\phi}{\partial x} = \sum \int_{x_\rho}^{x_t} \Delta C_{p_u}(\xi)\left(\frac{\partial\phi_1}{\partial x} + \frac{\partial\phi_2}{\partial x}\right)d\xi \tag{6}$$

where

$$\phi_1 = \frac{1}{8\pi} \int_L [(\frac{1}{r_1^2} + \frac{x_o}{Rr_1^2}) z_o \exp[-i\omega(u_1 r_1 + x_o)/v_\infty)] d\eta$$

$$\phi_2(x, y, z) = -\frac{i\omega}{V_\infty}\frac{1}{8\pi} \int_L \frac{z}{r_1^2} I(x, y, z, \xi, \eta) d\eta$$

$$I(x, y, z, \xi, \eta) = \int_{\tau_1 r_1}^{\infty} (1 - \frac{\tau'}{(\tau'^2 + r_1^2)^{1/2}}) \exp[-i\omega(\tau' + x_o)/V_\infty] d\tau' ,$$

$\sum$ denotes the summation overall spanwise strips, and x_p and x_t are the x coordinates of the leading and trailing edges, respectively, of the chord through the collocation (or control) points.

With the transformation

$$\xi = x_\ell + c(1 - \cos\theta)/2$$

equation (6) becomes

$$\frac{\partial\phi}{\partial z} (x, y, z) = \sum \frac{c}{2} \int_o^\pi \Delta C_{p_u}(\theta) \sin\theta (\frac{\partial\phi_1}{\partial z} + \frac{\partial\phi_2}{\partial z}) d\theta \tag{7}$$

etc.

Note that $\sin(\theta)$ cancels the square root singularities of ΔC_{p_u} at the leading and trailing edges. Therefore equation (5) can be reduced to a finite sum through the midpoint trapezoidal rule. Hence,

$$\frac{\partial\phi}{\partial z} (x,y,z) = \sum \frac{c\pi}{2N_c} \sum_{k=1}^{N_c} \Delta C_{p_u}(\theta_k) \sin\theta_k (\frac{\partial\phi_{1k}}{\partial z} + \frac{\partial\phi_{2k}}{\partial z}) \tag{8}$$

etc.

where N_c is the number of integration points and

$$\theta_k = (2k - 1)\pi/(2N_c).$$

The location of the "bounded" element of the oscillating horseshoe vortices is given by

$$\xi_k = x_\ell + \frac{c}{2} \{1 - \cos[(2k - 1)\pi/2N_c]\} , \ k = 1, \ldots, N_c$$

The x coordinates of end points of the bound elements are given by

$$x_{1k} = \xi_{1k},\ x_{2k} = \xi_{2k} \tag{9}$$

To eliminate the Cauchy singularity in the chordwise integral (ref. 4), a special set of control points is given:

$$\begin{aligned} x_c &= x_\ell + c[1 - \cos(i\pi/N_c)]/2 \qquad & i &= 1, \ldots, N_c \\ y_J &= b/2\{1 - \cos[J\pi/(N_s + 1)]\}/2 \qquad & j &= 1, \ldots, N_j \end{aligned} \tag{10}$$

where N_s is the number of spanwise strips.

Boundary Conditions

The boundary conditions for equation (2) are as follows: at an infinite distance from the surface disturbance potential should go to zero; and on the wing surface, the normal velocity component to the wing surface should be zero. Assuming that the wing surface can be described as

$$Z = z(x, y, t)$$

where Z is height above the plane, (Z = 0), of the wing surface. Assume that during oscillation every point of the wing moves in the vertical direction only. Thus, the velocity vector of a point on the wing is

$$\vec{w}_1 = \frac{\partial z}{\partial t}\hat{k} \tag{11}$$

The velocity vector of the fluid on the wing surface is

$$\vec{w}_2 = (U_\infty + u)\hat{i} + v\hat{j} + w\hat{k} \tag{12}$$

If these velocity vectors are resolved into tangential and normal components on the wing surface, and by applying the flow tangency condition, the following equation will be obtained:

$$\hat{n} = \frac{-\frac{\partial z}{\partial x}\hat{i} - \frac{\partial z}{\partial y}\hat{j} + \hat{k}}{\sqrt{1 + (\frac{\partial z}{\partial x})^2 + (\frac{\partial z}{\partial y})^2}} \tag{13}$$

$$\vec{w}_1 \cdot \hat{n} = \vec{w}_2 \cdot \hat{n} \tag{14}$$

by substituting (11), (12), and (13) into (14),

$$w = \frac{\partial z}{\partial t} + U_\infty \frac{\partial z}{\partial x} + v \frac{\partial z}{\partial y}$$

a. Longitudinal Motion

For a wing in plunging motion with displacement $\bar{h}(y, t)$, in pitching with angular displacement $\bar{\theta}(y, t)$ about $x = x_a$, and in rolling oscillations with roll angle $\bar{\phi}_r(t)$, the total vertical displacement $Z(x, y, t)$ is given by

$$Z(x, y, t) = -\bar{h}(y, t) - \bar{\theta}(y, t)(x - x_a) - y\bar{\phi}_r(t) \tag{15}$$

Note that $v \frac{dz}{dy}$ can be ignored because of small perturbation assumption.

$$\frac{\partial z}{\partial t} = -\bar{h} - \dot{\bar{\theta}}\,(x - x_a) - y\dot{\bar{\phi}}$$

$$\frac{\partial z}{\partial x} = -\bar{\theta}(y, t)$$

Hence, the nondimensional normal velocity is given by

$$w = -\frac{\dot{\bar{h}}}{U_\infty} - \frac{\dot{\bar{\theta}}}{U_\infty}(x - x_a) - y\dot{\bar{\phi}} - \bar{\theta} \tag{16}$$

Assuming the harmonic time variation such that

$$\bar{w}(x, y, t) = \mathrm{Re}[w(x, y)e^{i\omega t}], \text{ etc. },$$

equation (16) becomes

$$-w(x, y) = \Delta\alpha = \frac{ik}{\ell_r} h + \frac{ik}{\ell_r}\theta(x - x_a) + i\frac{k}{\ell_r} y\phi + \theta \tag{17}$$

The additional angle of attack ($\Delta\alpha$) is added to the steady angle of attack to produce the total normal velocity, (w_t) , which is (ref. 4)

$$w_t(x, y) = \frac{\partial z_c}{\partial x}\cos\alpha_s - \sin(\alpha_s + \Delta\alpha) \tag{18}$$

$$= \frac{\partial z_c}{\partial x}\cos\alpha_s - \sin\alpha_s - \Delta\alpha\cos\alpha_s$$

b. Lateral-Directional Motion:

For a wing in sideway motion with displacement d(t), and in yawing with angular displacement $\psi(\phi_o t)$ about $\eta = x_a$, the total side displacement Y is given by

$$F(x, y, z, t) = Y - f(x, z, t), \tag{19}$$

where

$$Y = -d(t) - \psi(t)(x - x_a)$$

Noting that

$$\frac{\partial\bar{f}}{\partial t} + U_\infty\frac{\partial\bar{f}}{\partial x} = v, \tag{20}$$

the following side velocity contribution from the motion of aircraft will be obtained:

$$\frac{v}{U_\infty} = -\frac{\dot{d}}{U_\infty} - \frac{\dot{\psi}}{U_\infty}(x - x_a) - \psi \tag{21}$$

If the wing has dihedral, the following normal velocity will appear in boundary conditions; otherwise, it will be zero.

$$\frac{w}{U_\infty}\cos\tau - \frac{v}{U_\infty}\sin\tau = -ik[\frac{d}{\ell_r}\sin\tau + \frac{\psi(x - x_a)}{\ell_r}\sin\tau] - \psi\sin\tau \qquad (22)$$

where τ is dihedral angle.

The total normal velocity can be canceled on the wing by using a steady horseshoe vortex distribution for the first two terms on the right-hand side of equation (18), and by a distribution of doublet for the last term in equations (18) and (22).

2.3 Free Vortex Filaments

A method similar to steady free vortex filament is used to model the unsteady leading-edge vortex separation. Here each vortex filament will be divided into many segments, and each segment will be called an oscillatory line vortex. The induced velocity due to an oscillatory line vortex of unit strength is derived in Appendix A. The resulting induced velocity components due to an oscillatory line vortex are given as follows:

$$\frac{\partial\phi}{\partial x} = \frac{\partial\phi_1}{\partial x} + \frac{\partial\phi_2}{\partial x}$$

$$\frac{\partial\phi}{\partial z} = \frac{\partial\phi_1}{\partial z} + \frac{\partial\phi_2}{\partial z}$$

$$\frac{\partial\phi}{\partial y} = \frac{\partial\phi_1}{\partial y} + \frac{\partial\phi_2}{\partial y} \qquad (23)$$

where:

$$\phi_1 = \frac{\Delta c_p}{8\pi} [(F_1 + F_3 - F_4)e^{-i\frac{\omega}{V}(\tau_1 r_1 + x_o)}\Big|_L -$$

$$\int_L (-\frac{i\omega}{V_\infty})F \frac{\partial}{\partial\eta}(\tau_1 r_1 + x_o)e^{-\frac{i\omega}{V}(\tau_1 r_1 + x_o)} d\eta]$$

$$F = \int (\frac{1}{r_1^2} + \frac{x_o}{Rr_1^2})z \; d\eta$$

$$F_1 = \int \frac{z_o}{r_1^2}\frac{x_o}{R} d\eta$$

$$F_3 = \text{Arctan} [\frac{z(x_1 - x)}{(y_1 - y)\sqrt{(x_1 - x)^2 + \beta^2(y_1 - y)^2 + \beta^2 z^2}}$$

$$F_4 = \text{Arctan} [\frac{z(x_2 - x)}{(y_2 - y)\sqrt{(x_2 - x)^2 + \beta^2(y_2 - y)^2 + \beta^2 z^2}}$$

$$\phi_2 = -\frac{i\omega}{V}\frac{1}{8\pi}\int_L \frac{z}{r_1^2} I(x, y, \xi, \eta)d\eta$$

where:

$$I = \int_{\tau_1 r_1}^{\infty} (1 - \frac{\tau'}{(\tau'^2 + r_1^2)^{1/2}})\exp[-i\omega(\tau' + x_o)/V_\infty]d\tau'$$

As mentioned before, small-amplitude harmonic motion is assumed. Therefore, the effects of oscillatory free vortex filaments and steady state free vortex filaments can be superimposed. In both cases the force-free condition on vortex filaments will be enforced. Also, partial separation along the leading edge is allowed (ref. 1).

Note that the derivation of equation (23) is based on the assumption that the vortex line is situated on the plane of $z = 0$. Therefore, the induced velocity is always calculated first with respect to a local plane of reference containing the vortex line; and the results are then transferred to the fixed plane of reference.

2.4 Method of Solution with Vortex Flow

The problem is resolved into steady and unsteady components, through harmonic assumption. Then after a known steady state solution is obtained, the solution for the unsteady motion will be calculated and superimposed to the mean steady flow. The basic unknowns of the problem are the strength of oscillatory horseshoe vortices, strength of oscillatory leading-edge vortices, and the locations of the free elements. The problem is nonlinear because the locations of the leading-edge vortices are unknown a priori. Therefore, the solution procedures based on an iterative method described below must be used:

a. Prescribe the doublet lattice for the wing surface, and the steady-state locations of the free elements over the wing.

b. By satisfying flow tangency condition on the wing surface, obtain the doublet and oscillatory leading-edge vortex strengths.

c. Calculate all the aerodynamic characteristics.

d. Enforce force-free condition on free elements by aligning them in the direction of local velocity vector.

e. Repeat steps b through d until a converged solution is obtained.

Note that typically the out-of-phase induced velocity on free vortex filaments is quite small compared to the free stream.
Therefore, $C_{\ell_{\dot{\beta}}}$ is calculated with the symmetric vortex shape. In addition, in the vortex-breakdown region, it is assumed that the phase angle is 90 deg, so that the in-phase force component without breakdown effect becomes out of phase, and vice versa.

2.5 Calculation of Aerodynamic Characteristics

The pressure distribution on lifting surfaces is calculated by applying unsteady compressible Bernoulli's equation (ref. 9), which has the following form:

$$\frac{\partial \phi}{\partial t} + \frac{\nabla\phi \cdot \nabla\phi}{2} + \int_{p_\infty}^{p} \frac{dp_1}{\rho_1} = \frac{U_\infty}{2} \tag{24}$$

By using the isentropic relation, definition of pressure coefficient, and finally linearizing the equation, the following relationship between pressure coefficient and velocity potential is derived (ref. 9):

$$c_p \simeq -\frac{2}{U_\infty}\frac{\partial \phi}{\partial x} - \frac{2}{U_\infty^2}\frac{\partial \phi}{\partial t} \tag{25}$$

To evaluate change in pressure coefficient, the relationship between velocity potential and circulation is used; then the

resulting equation in terms of vortex strength Γ becomes (ref. 9, p. 210)

$$\Delta\bar{c}_p = + \frac{2}{U_\infty^2} [\frac{\partial\bar{\Gamma}}{\partial t} + U_\infty \frac{\partial\bar{\Gamma}}{\partial x}] \quad (26)$$

To solve equation (26), harmonic approach is used, to transform the above partial differential equation (26) into a first-order ordinary nonhomogenous differential equation, in which the circulation amplitude is an unknown, i.e.:

$$\Delta c_p = \frac{2}{U_\infty^2} [i\omega\Gamma + U_\infty \frac{\partial\Gamma}{\partial x}] \quad (27)$$

The solution of Equation (27) is

$$\Gamma = \frac{U_\infty}{2} e^{-\frac{i\omega x}{U_\infty}} \int \Delta c_p e^{-\frac{i\omega x}{U_\infty}} dx \quad (28)$$

Finally, the lifting pressure due to oscillating bound elements and chordwise vortex elements, based upon the following relationship, will be obtained.

$$(\Delta c_p)_B = 2(u - v \tan\psi) \frac{\gamma}{U_\infty} + \frac{2ik}{\ell_r} \frac{\Gamma}{U_\infty} \quad (29)$$

$$(\Delta c_p)_T = 2\Gamma \frac{v}{U_\infty} + \frac{2ik}{\ell_r} \frac{\Gamma}{U_\infty} \quad (30)$$

Note that the calculated Δc_p is interpolated if necessary to obtain Δc_p at integration stations. The calculated pressure forces are then used to determine the aerodynamic characteristics in a way similar to the steady flow.

2.6 Longitudinal Dynamic Stability Derivatives

In general, the amplitudes of lift and pitching moment coefficients in oscillatory motion can be expressed in terms of stability derivatives as follows (ref. 10)

$$C_N = ik \frac{h}{\ell_r} C_{N_{\dot{h}}} - k^2 C_{N_{\ddot{h}}} \frac{h}{\ell_r} + \theta C_{N_\theta} + ik\theta C_{N_{\dot{\theta}}} + \ldots \qquad (31)$$

$$C_m = ik \frac{h}{\ell_r} C_{m_{\dot{h}}} - k^2 C_{m_{\ddot{h}}} \frac{h}{\ell_r} + \theta C_{m_\theta} + ik\theta C_{m_{\dot{\theta}}} + \ldots \qquad (32)$$

At zero frequency, $C_{m_\theta} = C_{m_\alpha}$; and at small frequencies,

$$C_{m_{\dot{\theta}}} = C_{m_q} + C_{m_{\dot{\alpha}}} \qquad (33)$$

where $C_{m_{\dot{\alpha}}}$ can be shown to be equal to $C_{m_{\ddot{h}}}$.

2.7 Lateral Dynamic Stability Derivatives

In a similar approach as in the longitudinal case, the amplitudes of side forces, and rolling and yawing moment coefficients, in each mode of oscillatory motion are expressed in terms of stability derivatives. The results are as follows:

a. Sideslipping ($\beta = \dot{d}$)

$$C_y = ik(C_{y_\beta} - k^2 C_{y_{\ddot{\beta}}})d - k^2 C_{y_{\dot{\beta}}} \qquad (34)$$

$$C_n = ik(C_{n_{\ddot{\beta}}})d - k^2 d C_{n_{\dot{\beta}}} \qquad (35)$$

$$C_\ell = ik(C_{\ell_\beta} - k^2 C_{\ell_{\ddot{\beta}}})d - k^2 d C_{\ell_{\dot{\beta}}} \qquad (36)$$

b. **Rolling Motion** ($p = \dot{\phi}$)

$$C_y = ik\phi(C_{y_p} - k^2 C_{y_{\ddot{p}}}) - k^2\phi C_{y_{\dot{p}}} + \phi C_{y_\phi} \tag{37}$$

$$C_n = ik\phi(C_{n_p} - k^2 C_{n_{\ddot{p}}}) - k^2\phi C_{n_{\dot{p}}} + \phi C_{n_\phi} \tag{38}$$

$$C_\ell = ik\phi(C_{\ell_p} - k^2 C_{\ell_{\ddot{p}}}) - k^2\phi C_{\ell_{\dot{p}}} + \phi C_{\ell_p} \tag{39}$$

c. **Yawing Motion** ($r = \dot{\psi}$)

$$C_y = ik\psi(C_{y_r} - k^2 C_{y_{\ddot{r}}}) - k^2\psi C_{y_{\dot{r}}} + \psi C_{y_\psi} \tag{40}$$

$$C_n = ik\psi(C_{n_r} - k^2 C_{n_{\ddot{r}}}) - k^2\psi C_{n_{\dot{r}}} + \psi C_{n_\psi} \tag{41}$$

$$C_\ell = ik\psi(C_{\ell_r} - k^2 C_{\ell_{\ddot{r}}}) - k^2\psi C_{\ell_{\dot{r}}} + \psi C_{\ell_\psi} \tag{42}$$

2.8 Dynamic Stall Effect

Dynamic stall effect is important in predicting dynamic stability parameters for configurations with low-swept wing planforms. Since theoretical calculations are very time-consuming and may not be accurate, it is proposed to calculate three-dimensional results by using 2-D test data. The concept is quite similar to that in steady flow to account for the effect of boundary layer separation (ref. 1). That is, iterative calculation is first made for steady separation effect to obtain local effective angles of attack (α_e). Local effective oscillation amplitudes are calculated by using a three-dimensional unsteady attached-flow

method (ref. 4). Two-dimensional test data are interpolated based on these local effective angles of attack and oscillation amplitudes. To interpolate, the 2-D test data must be expressed in terms of nonlinear functions of α_1 and $\dot{\alpha}_1$, which depends on oscillation amplitudes. This is done by Fourier analysis. The resulting mean value is a function of mean angles of attack (α_m) which are interpolated for the appropriate sets of data to be used at the calculated α_e. One set of calculations will be illustrated later to expose this idea.

3. NUMERICAL RESULTS AND DISCUSSION

In the following, calculated results for delta wings with sweep angles of 60° and 80° will be presented. In addition, calculated results for the F-106B configuration will be compared with data. All calculations are made in eight iterations to adjust free vortex positions. The vortex breakdown effect is applied only at the last iteration. Finally, calculated results for a rectangular wing with dynamic stall effect will be illustrated.

Delta Wing with a Sweep Angle of 60°

Lateral coefficients for this configuration are presented in Fig. 1. The aerodynamic characteristics are significantly influenced by free vortex position, the motion lag, and the bursting locations. Typically, $C_{\ell_{\dot{\beta}}}$ is positive without vortex breakdown and becomes negative only with vortex bursting. As it can be seen, due to early vortex breakdown for this configuration, the resulting rolling moment coefficients due to $\dot{\beta}$ become largely negative and cause the roll damping derivatives to be more negative. Also as α is increased, the effect of $\dot{\beta}$ derivatives due to lag in motion is more appreciable. As the reduced frequency is increased, the magnitude of $C_{\ell_{\dot{\beta}}}$ will diminish but still is negative. The test data indicate that vortex bursting occurred at a lower α than the calculated value which was based on a steady-flow model. It should also be noted that the vortex bursting point is known to be affected by dynamic motion. Since a systematic set of data is not available,

the dynamic effect on vortex bursting cannot be assessed at the present time.

The discrepancy between the calculated results and experiments is mainly due to prediction of vortex breakdown location.

Delta Wing with a Sweep Angle of 80°

Lateral-directional derivatives for this configuration are determined at a reduced frequency of 0.06 and an amplitude of 5°. The calculated results show large positive rolling moment coefficients due to $\dot{\beta}$ (see Fig. 2). For this configuration, the vortex breakdown occurs at about $\alpha = 38°$. Therefore, this positive rolling moment due to $\dot{\beta}$ causes C_{ℓ_p} to be more positive, which may result in wing rock. The correlation between the experimental data and numerical results is good. At high angles of attack, the effect of $\dot{\beta}$ derivatives is more significant and is therefore important to dynamic stability of airplanes, in particular those with highly swept wings. The present numerical results show that the acceleration derivatives can be predicted within a reasonable accuracy for highly swept wings. Also, in a forced-oscillation test, it is not possible to decouple the effect of $\dot{\beta}$ from the P motion. However, by the present method, it is possible to decouple the effect of each mode separately.

F-106B Configuration

This configuration has a conically cambered wing of 60-deg sweep and a vertical tail. At a reduced frequency of 0.2, the factor for the remaining vortex lift after breakdown is not applied, since not enough data on dynamic vortex breakdown are available for guidance. The calculated results are presented in Fig. 3(a) for roll stability derivatives and in Fig. 3(b) for yaw derivatives. It is seen from Fig. 3 that predicted roll and yawing moment derivatives are significantly improved by including $\dot{\beta}$-derivatives. Note that $C_{y_{\dot{\beta}}}$ at $\alpha = 35$ deg is quite negative and is contributed by the vertical tail. Since the dynamic fuselage effect is not available in the current version of the code, it is not known whether it will improve the predicted results at $\alpha = 35$ deg.

Rectangular Wing of Aspect Ratio 4 with Dynamic Stall Effect

Some dynamic stall data on several airfoil sections are available in reference 11. However, only data for the NACA 0012 airfoil are more complete and therefore will be used in the following. This set of data was obtained by oscillating the airfoil about the quarter-chord point at mean angles of attack (α_m) of 3, 4, 5, and 10 degs and an amplitude α_1 of 10 deg at a reduced frequency $(\omega c/2V_\infty) = 0.1$ and a Mach number of 0.3. The sectional $c_\ell - \alpha$ curves are presented in Figure 4. These sectional data are then analyzed through Fourier analysis to obtain c_ℓ as functions of α_1 and $\dot{\alpha}_1$. For example, at $\alpha_m = 5$ deg, c_ℓ can be written as

$$c_\ell = 0.4825 + (5.114 + 1.184\alpha_1 + 5.198\alpha_1^2 + 79.694\alpha_1^3$$

$$+ 42.474\alpha_1^4 - 0.005\dot{\alpha}_1^2 - 0.2298\alpha_1\dot{\alpha}_1^2 - 0.245\alpha_1^2\dot{\alpha}_1^2)\alpha_1$$

$$+ (0.007 + 0.0979\alpha_1 - 0.051\alpha_1^2 - 2.171\alpha_1^3 - 7.149\alpha_1^4$$

$$+ 0.006\alpha_1\dot{\alpha}_1^2 + 0.0412\alpha_1^2\dot{\alpha}_1^2 - 0.001\dot{\alpha}_1 - 0.0328\alpha_1^2\dot{\alpha}_1)\dot{\alpha}_1 \qquad (43)$$

where the constant term on the right-hand side is the mean value of c_ℓ (i.e. c_{ℓ_m}). In the calculation for a wing, this c_{ℓ_m} is linearly interpolated with the effective angle of attack. In Figure 5, the calculated aerodynamic models at α_m equal to 5 and 10 deg are compared with data. The agreement is reasonably good.

Assume that a rectangular wing of aspect ratio 4 and with the NACA 0012 airfoil section is oscillated in pitch about the quarter chord point with the same flow conditions as those used in the airfoil testing. The resulting total $C_L - \alpha$ curve is plotted in Figure 6 and calculated sectional c_ℓ's at three spanwise stations are illustrated in Figure 7. Since there are no experimental data for the wing available for comparison, no assessment of accuracy can be offered. However, the results appear to be plausible. Note that calculated c_ℓ and C_L do not pass through the coordinate origin. This discrepancy is caused by the assumption of linear interpolation of c_{ℓ_m} with respect to the effective angle of attack. Except having this discrepancy, Eq. (43) and other similar equations not listed here appear to be capable of modeling the dynamic stall effect at different amplitudes and mean angles of attack.

In applications to fighter configurations, dynamic stall data of typical thin airfoils are needed. These data can then be used to predict dynamic effect on longitudinal and lateral-directional aerodynamic characteristics.

4. CONCLUSIONS

An unsteady, compressible, aerodynamic method was developed to calculate dynamic stability parameters at high angles of attack. In the method, the edge-separated vortex flow was represented by free-vortex filaments in frequency domain. The main emphasis of the method was to calculate dynamic lateral-directional stability parameters. Calculated results of $C_{\ell_{\dot{\beta}}}$ for a delta wing of 80 degs were shown to produce total roll damping derivatives which agreed well with data. For the 60-deg delta wing, the calculated trend of $C_{\ell_{\dot{\beta}}}$ variation with α is correct, except that its magnitude is lower at low α than the data showed. Calculated results for an F-106B configuration with the unsteady method show significant improvement in predicting dynamic roll and yaw stability derivatives.

Calculation of dynamic stall effect for a rectangular wing of aspect ratio 4 was also demonstrated. The calculation was based on interpolation of two-dimensional test data at the calculated sectional effective angles of attack. No 3-D data were available for comparison. However, the calculated results appeared plausible.

5. RECOMMENDATIONS

This investigation represents an initial attempt to predict dynamic effect on aerodynamic characteristics at high angles of attack. To improve the prediction method, the following experimental and theoretical work would be needed.

(1) Obtain experimentally a systematic set of dynamic stall data in c_ℓ, c_d, c_m on a thin airfoil typical of current fighter wings. This set of data can be used in the present method to calculate dynamic stability derivatives on wings with low sweep angle.

(2) Obtain experimentally a systematic set of dynamic vortex breakdown data on delta wings of different sweep angles. The data should include the dynamic effect on bursting position and total lift variation. This set of data will be analyzed and incorporated into the present method to calculate dynamic stability derivatives on wings with high sweep angle.

(3) Develop an unsteady mathematical model to represent the fuselage effect.

6. REFERENCES

1. Lan, C. E.; Emdad, H.; Chin, S; Sundaram, P.; and Mehrotra, S. C. "Calculation of High Angle-of-Attack Aerodynamics of Fighter Configurations." AIAA Paper 89-2188, August 1989.
2. Nguyen, L. T. "Evaluation of Importance of Lateral Acceleration Derivatives in Extraction of Lateral-Directional Derivatives at High Angles of Attack." NASA TN D-7739, 1974.
3. Orlik-Rückmann, K. J. "Aerodynamic Aspects of Aircraft Dynamics at High Angles of Attack." AIAA Paper 82-1363, August 1982.
4. Lan, C. E. "The Unsteady Suction Analogy and Applications." AIAA Journal, Vol. 20, No. 12, Dec. 1982, pp. 1647-1656.
5. Atta, E. H.; Kandil, O. A.; Mook, D. T.; and Nayfeh, A. H. "Unsteady Aerodynamic Loads on Arbitrary Wings Including Wing-Tip and Leading-Edge Separation." AIAA Paper No. 77-156, 1977.
6. Nayfeh, A. H.; Mook, D. T.; and Yen, A. "The Aerodynamics of Small Harmonic Oscillations around Large Angles of Attack." AIAA Paper 79- 1520, July 1979.
7. Levin, D.; and Katz, J. "A Vortex-Lattice Method for the Calculation of the Nonsteady Separated Flow over Delta Wings." AIAA Paper 80-1803, August 1980.
8. McCroskey, W. J. "The Phenomenon of Dynamic Stall." NASA TM 81264, March 1981.
9. Dowell, E. H., et al. Modern Course in Aeroelasticity. Sijthoff and Noordhoff International Publisher, 1978.

10. Rodden, W. P.; and Giesing, J. P. "Application of Oscillatory Aerodynamic Theory to Estimation of Dynamic Stability Derivatives." Journal of Aircraft, Vol. 7, May-June 1970, pp. 272-275.

11. McCroskey, W. J.; McAlister, K. W.; Carr, L. W.; Pucci, S. L.; Lambert, O.; and Indergrand, R. F. "Dynamic Stall on Advanced Airfoil Sections." Journal of the American Helicopter Society, Vol. 26, July 1981, pp. 40-50.

12. Lichtenstein, J. H.; and Williams, J. L. "Effect of Frequency of Sideslipping Motion on the Lateral Stability Derivatives of a Typical Delta Wing Airplane." NACA RM L57F07, 1957.

13. Nguyen, L. T.; and Chambers, J. R. "Self-Induced Wing Rock of Slender Delta Wings." AIAA Paper No. 81-1883, 1981.

14. Yip, L. P. "Wind-Tunnel Free-Flight Investigation of a 0.15-Scale Model of the F-106B Airplane with Vortex Flaps." NASA TP-2700, 1987.

15. Jordon, P. "Numerical Evaluation of the Three-Dimensional Harmonic Kernel." Zeitschrift für Flugwissenschaften, Vol 24, 1976, pp. 205-209.

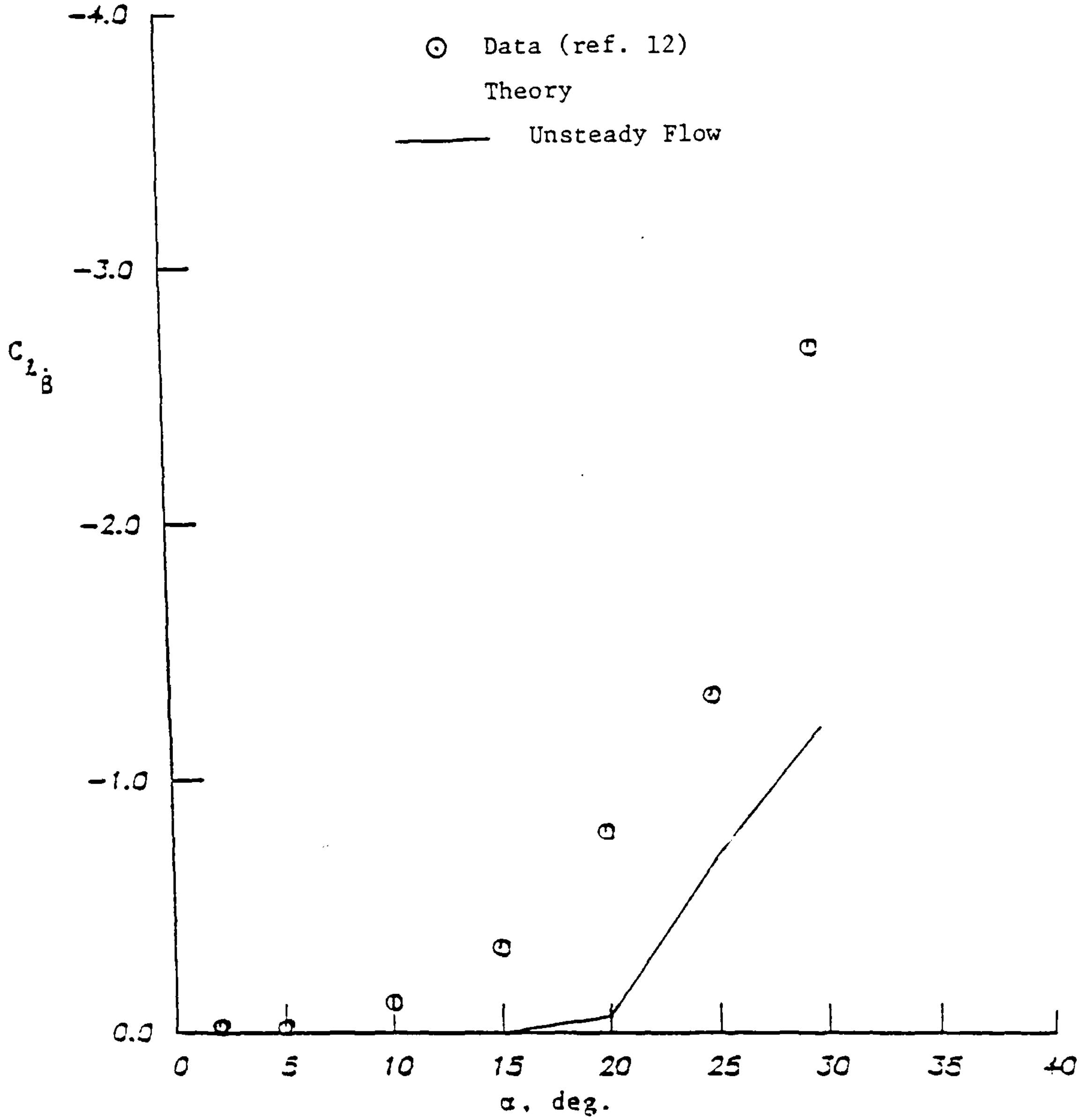

Figure 1 Rolling Moment Coefficient due to Side Acceleration for a 60-deg Delta Wing at M = 0.13, k = 0.066 and Amplitude = 5 deg.

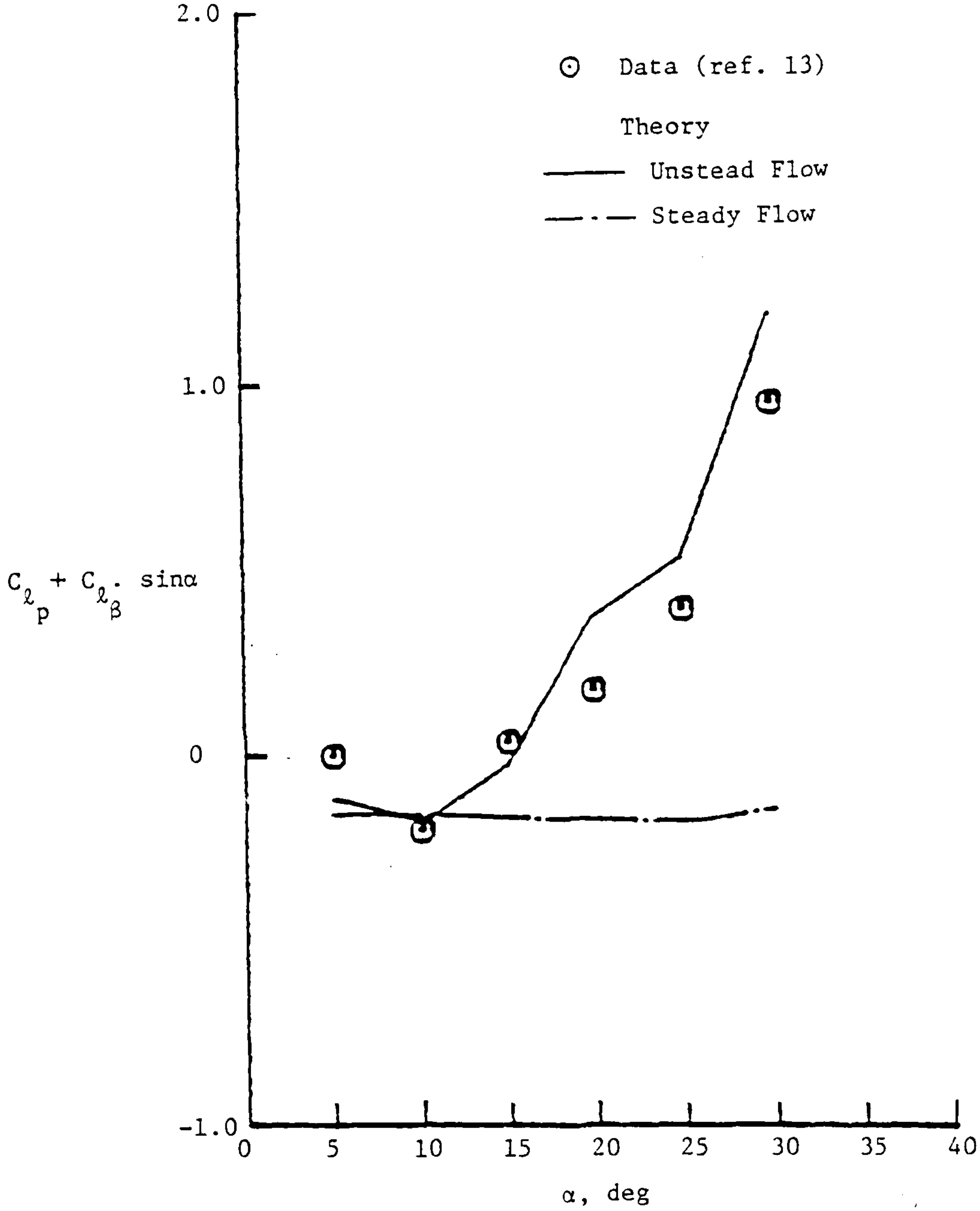

Figure 2 Roll Damping Derivatives of an 80-deg Delta Wing at M = 0.1, k = 0.06 and Amplitude = 10 deg.

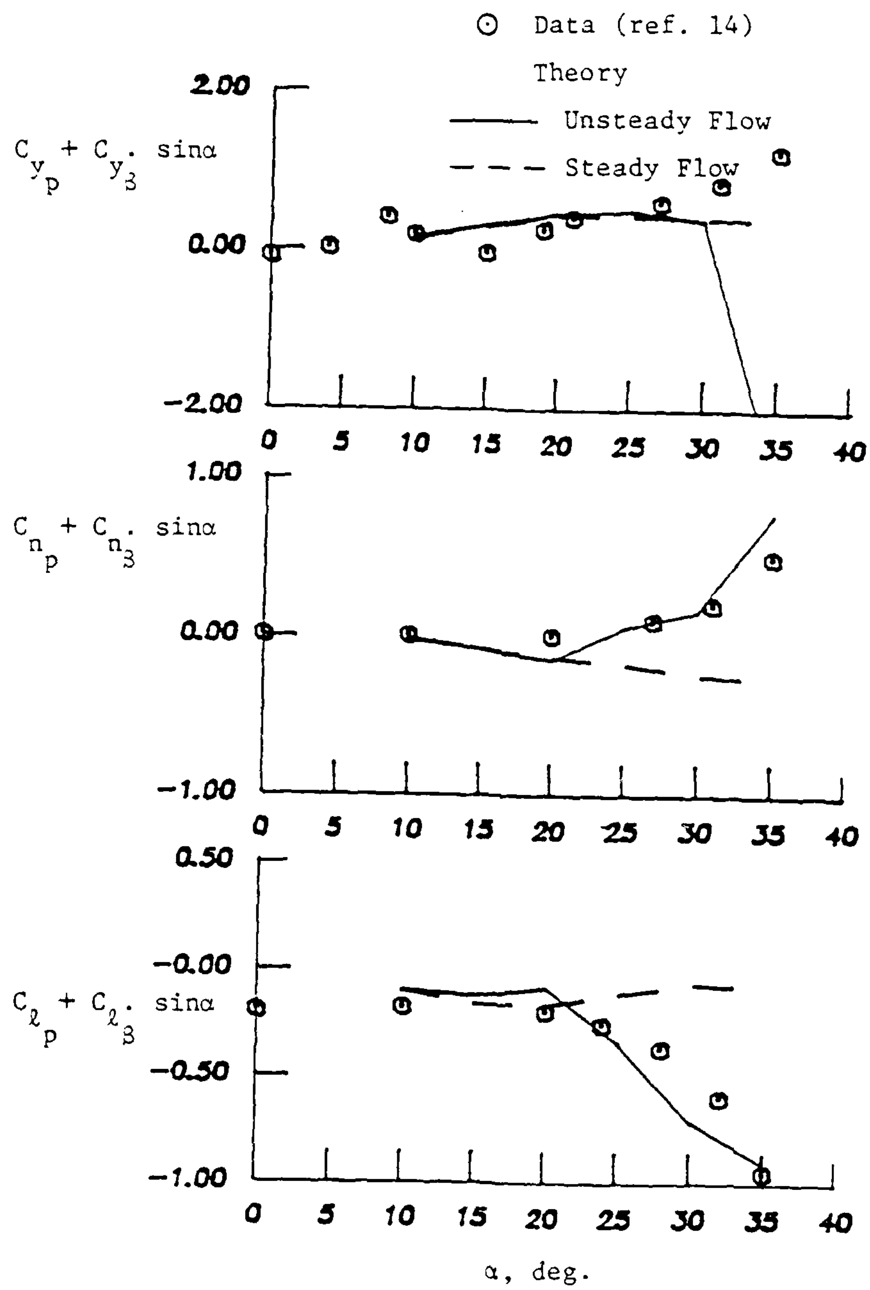

(a) Roll Derivatives

Figure 3 Dynamic Stability Derivatives for an F-106B Configuration at $M = 0.1$ and $k = 0.2$. Moment Center at $0.275\,\bar{c}$.

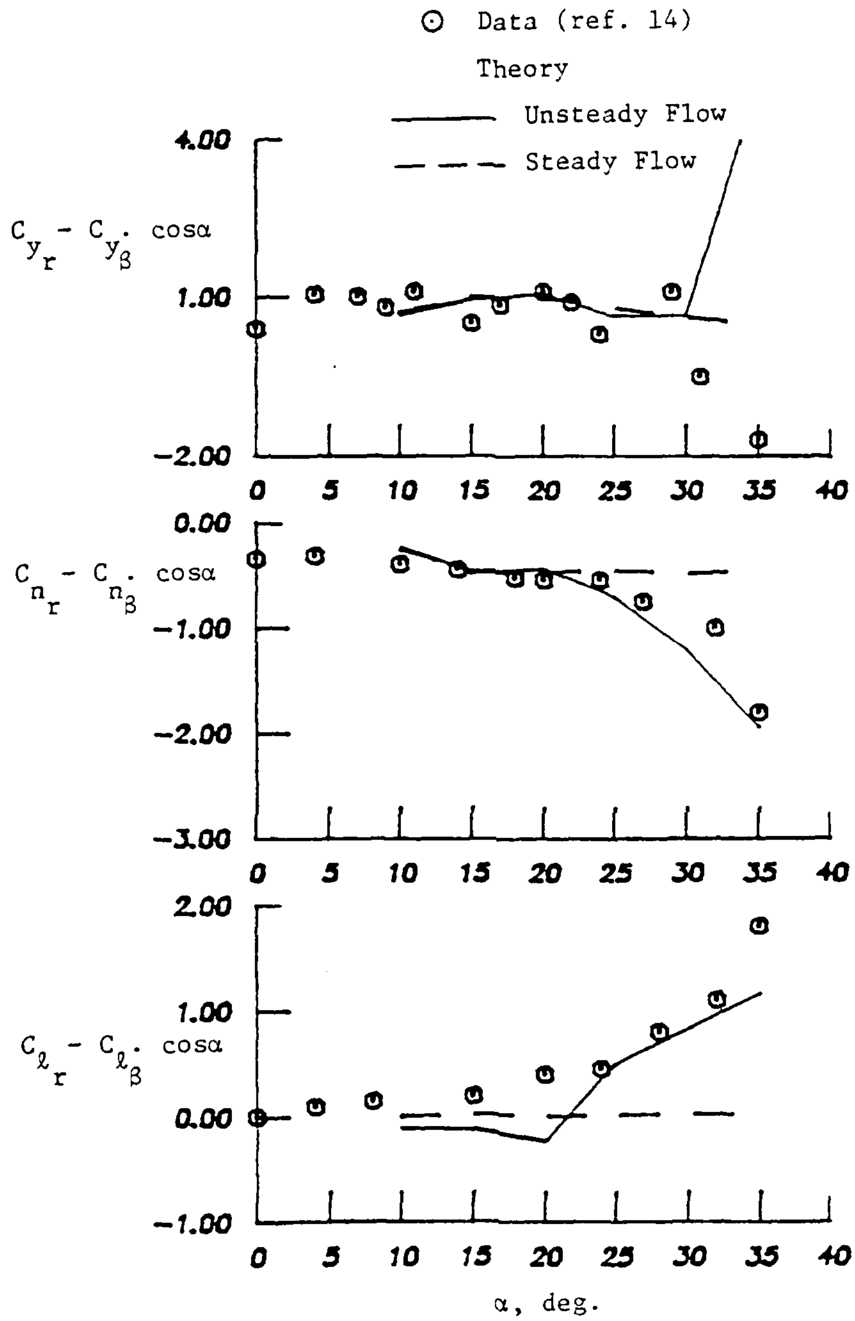

(b) Yaw Derivatives

Figure 3 Concluded.

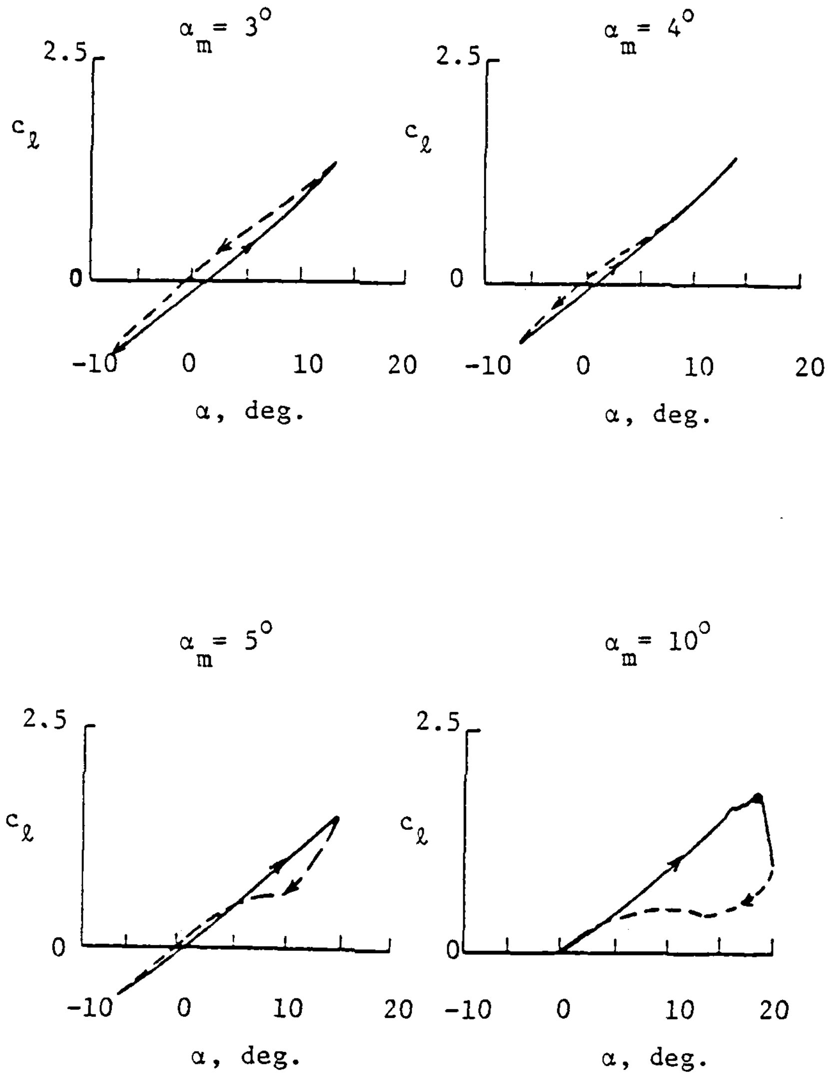

Figure 4 Measured Dynamic Stall Effect on Lift Curves on NACA 0012 Airfoil. $\alpha = \alpha_m + 10^\circ \sin\omega t$, $k = 0.1$ and $M = 0.3$ (ref. 11).

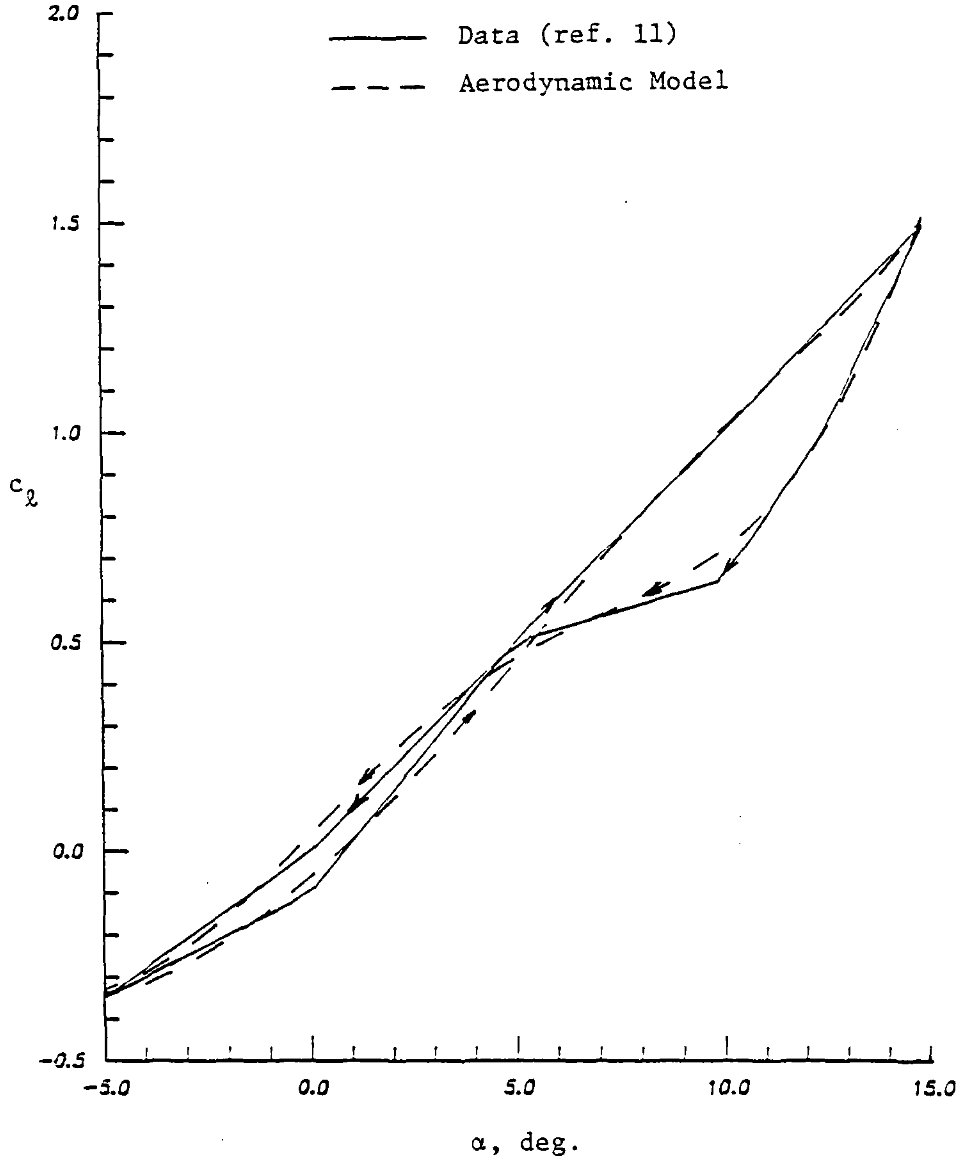

(a) $\alpha_m = 5$ deg.

Figure 5 Aerodynamic Models for an NACA 0012 Airfoil in Dynamic Stall Obtained from Figure 4.

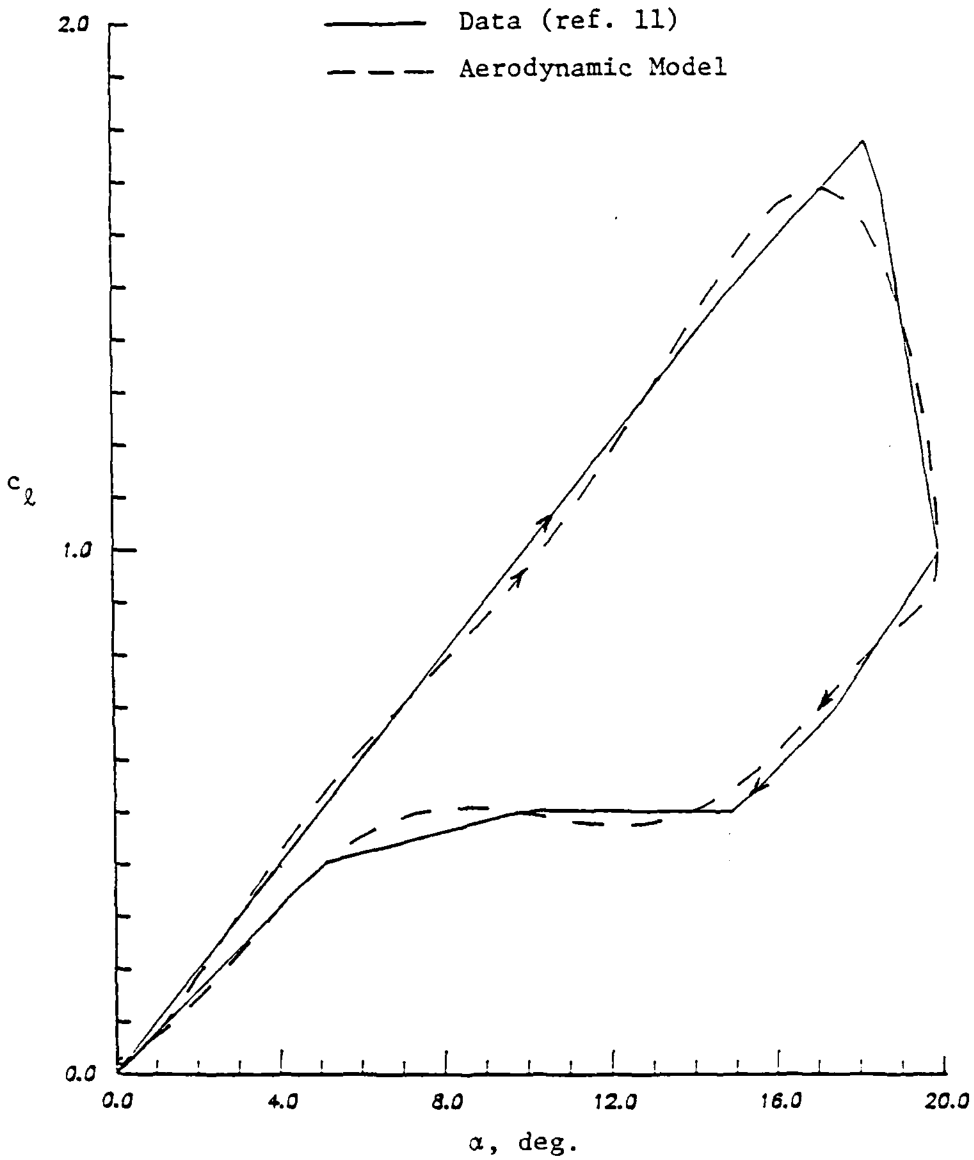

(b) $\alpha_m = 10$ deg.

Figure 5 Concluded.

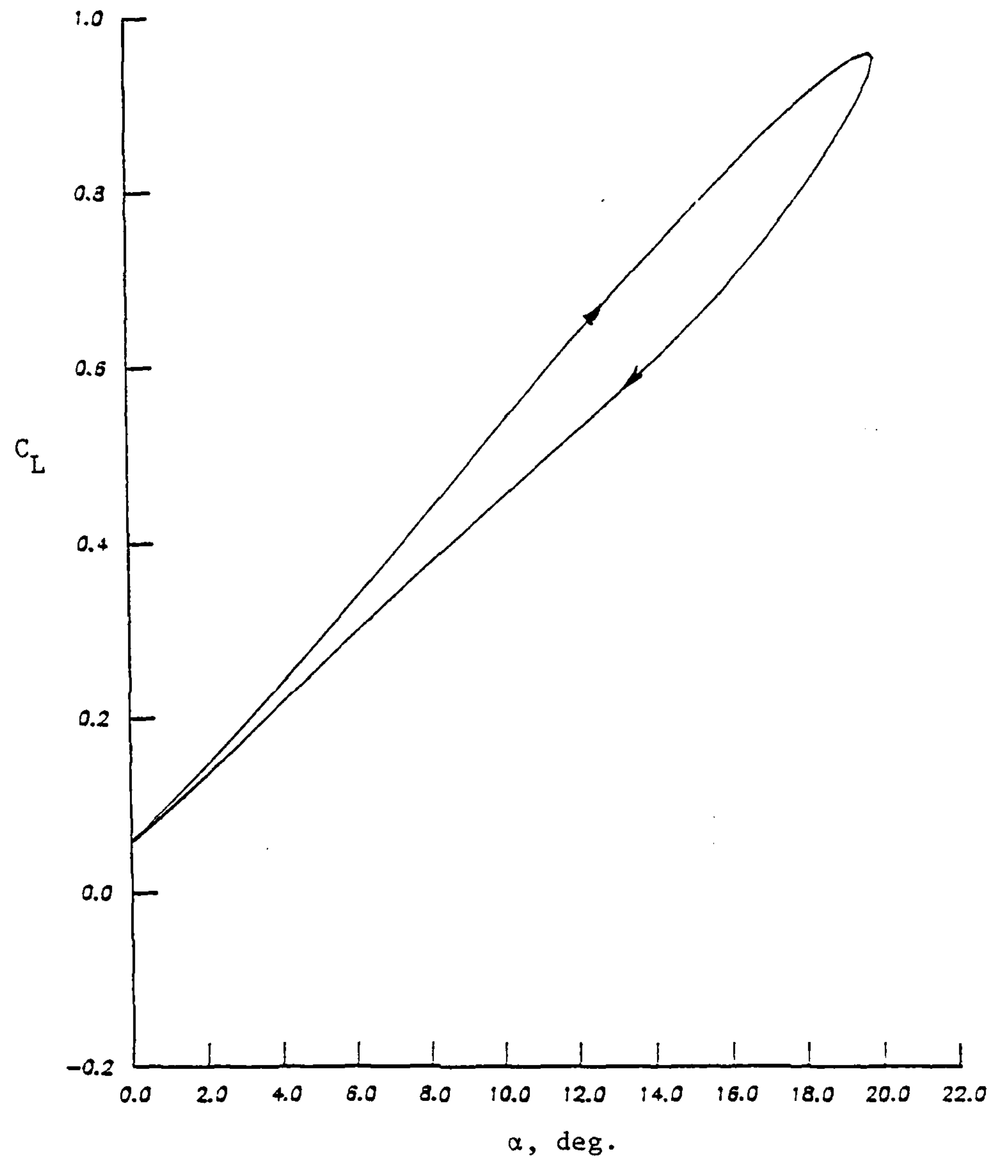

Figure 6 Calculated Lift Response on a Rectangular Wing of Aspect Ratio 4 with NACA 0012 Airfoil in a Pitching Oscillation about 1/4c at M = 0.3 anf k ≐ 0.1. $\alpha = 10^{\circ} + 10^{\circ} \sin\omega t$.

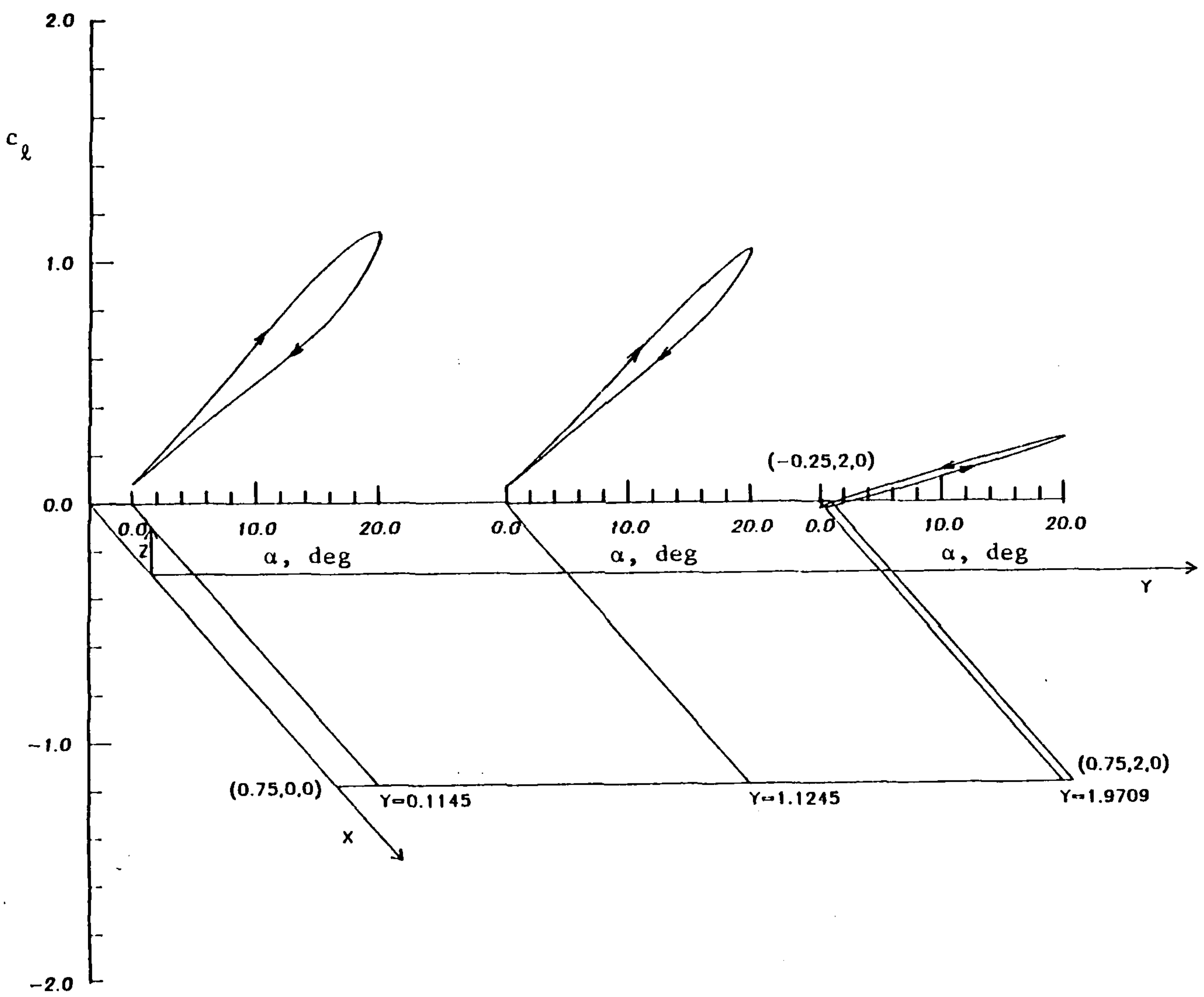

Figure 7 Calculated Sectional Lift Response at Three Spanwise Stations on a Rectangular Wing of Aspect Ratio 4 in Pitching Oscillation about 1/4 c at M = 0.3 and k = 0.1. $\alpha = 10^{\circ} + 10^{\circ} \sin\omega t$.

APPENDIX A:

DERIVATION OF INDUCED VELOCITY DUE TO AN OSCILLATING LINE VORTEX

The expression for induced velocities due to an oscillating horseshoe vortex are available. To obtain the corresponding expressions for an oscillating line vortex in compressible flow, the effect of trailing legs in the horseshoe vortex must be removed. To achieve this objective, the general equation for oscillating doublets is needed (ref. 4):

$$\frac{\phi}{V_\infty} = \frac{1}{8\pi} \iint_S \Delta C_p \{ (\frac{1}{r_1^2} + \frac{x_o}{Rr_1^2}) z_o \exp[-\frac{i\omega}{V}(\tau_1 r_1 + x_o)] -$$

$$\frac{i\omega}{V_\infty} \frac{z_o}{r_1} e^{-\frac{i\omega}{V_\infty} x_o} \int_{\tau_1}^{\infty} (1 - \frac{\lambda}{\sqrt{1+\lambda^2}}) e^{-\frac{i\omega r_1 \lambda}{V_\infty}} d\lambda \} d\xi d\eta \qquad (A.1)$$

Define:

$$\phi_1 = \frac{\Delta C_p}{8\pi} \int_L (\frac{1}{r_1^2} + \frac{x_o}{Rr_1^2}) z_o \exp[-\frac{i\omega}{V_\infty}(\tau_1 r_1 + x_o)] d\eta \qquad (A.2)$$

$$\phi_2 = \frac{\Delta C_p}{8\pi} \int_L [-\frac{i\omega}{V_\infty} \frac{z_o}{r_1} e^{-\frac{i\omega}{V_\infty} x_o} \int_{\tau_1}^{\infty} (1 - \frac{\lambda}{\sqrt{1+\lambda^2}}) e^{-\frac{i\omega}{V_\infty} r_1 \lambda} d\lambda] \qquad (A.3)$$

By integration by parts, equation (A.2) becomes

$$\phi_1 = \frac{\Delta C_p}{8\pi} \{ F \exp[-\frac{i\omega}{V_\infty}(\tau_1 r_1 + x_o)] \Big|_L - \int_L (-\frac{i\omega}{V_\infty}) F \frac{\partial}{\partial \eta}(\tau_1 r_1 + x_o) *$$

$$\exp[-\frac{i\omega}{V_\infty}(\tau_1 r_1 + x_o)] d\eta \} \qquad (A.4)$$

where:

$$r_1 = \sqrt{(y_o^2 + z_o^2} \; , \; \tau_1 = \frac{-x_o + M\sqrt{x_o^2 + \beta^2 r_1^2}}{\beta^2} \; , \; R = \sqrt{x_o^2 + \beta^2 y_o^2 + \beta^2 z_o^2}$$

$$F = \int_L \left(\frac{1}{r_1^2} + \frac{x_o}{Rr_1^2}\right) z_o \, d\eta \tag{A.5}$$

$$x_o = x - \xi = x - x_1 - \tau(x_2 - x_1)$$

$$y_o = y - \eta = y - y_1 - \tau(y_2 - y_1)$$

The straight line L is now defined by (0, 1) in τ (see Fig. A.1).

If F in the first term of equation (A.4) is replaced by the following form, equation (A.4) is reduced to oscillating line vortex:

$$F = \int_L \left(\frac{x_o}{Rr_1^2}\right) z_o \, d\eta + \text{Arctan}\left[\frac{z(x_1 - x)}{(y_1 - y)\sqrt{(x_1 - x)^2 + \beta^2 (y_1 - y)^2 + \beta^2 z^2)}}\right]$$

$$- \text{Arctan}\left[\frac{z(x_2 - x)}{(y_2 - y)\sqrt{(x_2 - x)^2 + \beta^2 (y_2 - y)^2 + \beta^2 z^2}}\right] \tag{A.6}$$

ϕ_1 is differentiated with respect to z with equation (A.6) for F and letting the frequency go to zero, the exact steady expression for a line vortex element can be obtained as will be shown later. Now consider the following expression in ϕ_2; i.e.,

$$I = \int_{\tau_1}^{\infty} \left(1 - \frac{\lambda}{\sqrt{1 + \lambda^2}}\right) e^{-\frac{i\omega}{V_\infty} r_1 \lambda} \, d\lambda \tag{A.7}$$

where:

$$\tau_1 = \frac{-x_o + M\sqrt{x_o^2 + r_1^2 \beta^2}}{\beta^2} \tag{A.8}$$

and $x_o = x - x_1$ or $x_o = x - x_2$

Let x_1 or x_2 in equation (A.7) go to infinity; hence:

$$\lim_{x_1 \to \infty} I = \lim_{x_1 \to \infty} \int_{\frac{-(x-x_1) + M\sqrt{(x-x_1)^2 + \beta^2 r_1^2}}{\beta^2}}^{\infty} \left(1 - \frac{\lambda}{\sqrt{1+\lambda^2}}\right) e^{-\frac{i\omega}{V_\infty} r_1 \lambda} \, d\lambda \tag{A.9}$$

The lower limit of integration goes to positive infinity as x_1 or x_2 goes to infinity; therefore,

$$\lim_{\substack{x_1 \to \infty \\ x_2 \to \infty}} I = 0$$

Therefore, it can be concluded that ϕ_2 is due to vortex shedding only and comes only from bound vortex of oscillating horseshoe vortex. Thus, the equation for an oscillating line vortex becomes:

$$\frac{\phi}{V_\infty} = \phi_1 + \phi_2 \tag{A.10}$$

where ϕ_1 and ϕ_2 are given by equations (A.6) and (A.3).

To derive expressions for induced velocities due to an oscillating line vortex, equation (A.10) is differentiated with respect to x, y, and z, respectively.

$$u = \frac{1}{V_\infty} \frac{\partial \phi}{\partial x} = \frac{\partial \phi_1}{\partial x} + \frac{\partial \phi_2}{\partial x} \tag{A.11}$$

$$v = \frac{1}{V_\infty} \frac{\partial \phi}{\partial y} = \frac{\partial \phi_1}{\partial y} + \frac{\partial \phi_2}{\partial y} \tag{A.12}$$

$$w = \frac{1}{V_\infty} \frac{\partial \phi}{\partial z} = \frac{\partial \phi_1}{\partial z} + \frac{\partial \phi_2}{\partial z} \tag{A.13}$$

Expressions from ϕ_1:

$$\phi_1 = \frac{\Delta C_p}{8\pi} \{F_1 e^{-\frac{i\omega}{V_\infty}(\tau_1 r_1 + x_o)} \Big|_L - \int_L (-\frac{i\omega}{V_\infty}) F \frac{\partial}{\partial\eta}(\tau_1 r_1 + x_o) \exp[-\frac{i\omega}{V_\infty}(\tau_1 r_1 + x_o)] d\eta\}$$

where:

$$F = \int_L (\frac{1}{r_1^2} + \frac{x_o}{Rr_1^2}) z_o d\eta$$

$$F = \int_L (\frac{x_o}{Rr_1^2}) z_o d\eta + \mathrm{Tan}^{-1}[\frac{z(x_1 - x)}{(y - y_1)\sqrt{(x_1 - x)^2 + \beta^2 (y_1 - y)^2 + \beta^2 z_o^2}}]$$

$$- \mathrm{Tan}^{-1}[\frac{z(x_2 - x)}{(y_2 - y)\sqrt{(x_2 - x)^2 + \beta^2 (y_2 - y)^2 + \beta^2 z^2}}]$$

Taking the derivative of ϕ_1 with respect to z results in

$$\frac{\partial\phi_1}{\partial z} = \frac{\Delta C_p}{8\pi} \{\frac{\partial F_1}{\partial z} e^{-\frac{i\omega}{V_\infty}(\tau_1 r_1 + x_o)} \Big|_L - (F_1 e^{-\frac{i\omega}{V_\infty}(\tau_1 r_1 + x_o)} \Big|(-\frac{i\omega}{V_\infty})(\tau_1 r_1 + x_o)\Big|_L -$$

$$\int_L (-\frac{i\omega}{V_\infty} (\frac{\partial F}{\partial z}) \frac{\partial}{\partial\eta} [(\tau_1 r_1 + x_o)] e^{-\frac{i\omega}{V_\infty}(\tau_1 r_1 + x_o)} d\eta -$$

$$\int_L (-\frac{i\omega}{V_\infty}) F \frac{\partial}{\partial\eta} [\frac{\partial}{\partial z}(\tau_1 r_1 + x_o)] e^{-\frac{i\omega}{V_\infty}(\tau_1 r_1 + x_o)} d\eta -$$

$$\int_L (-\frac{i\omega}{V_\infty})(F) \frac{\partial}{\partial\eta}(\tau_1 r_1 + x_o)(-\frac{i\omega}{V_\infty} \frac{\partial}{\partial z}(\tau_1 r_1 + x_o) e^{-\frac{i\omega}{V_\infty}(\tau_1 r_1 + x_o)} d\eta\} \tag{A.14}$$

where:

$$\frac{\partial F}{\partial z} e^{-\frac{i\omega}{V}(\tau_1 r_1 + x_o)}\Big|_L$$

$$= \frac{1}{\sqrt{(x-x_2)^2+\beta^2(y-y_2^2)+\beta^2(z^2)}} [Q \frac{(x_2-x)(x_2-x_1)+\beta^2(y_2-y_1)(y_2-y)+\beta^2 z}{Q^2 + z^2[(x_2+x_1)^2+ \beta^2(y_2-y_1)^2}]$$

$$* \exp [- \frac{i\omega}{V_\infty} \frac{M\sqrt{(x-x_2)^2+\beta^2(y-y)^2+\beta^2 z^2} - M^2(x-x_2)}{\beta^2} -$$

$$\frac{1}{\sqrt{(x-x_1)^2+\beta^2(y-y_1)^2+\beta^2(z-z_1)^2}} [Q \frac{(x_1-x)(x_2-x_1)+\beta^2(y_2-y_1)(y_1-y)+\beta^2 z}{Q^2+z^2[(x_2-x_1)+\beta^2(y_2-y_1)^2]} *$$

$$\exp \{- \frac{i\omega}{V_\infty} [\frac{M\sqrt{(x-x_1)^2+\beta^2(y-y_1)^2+\beta^2 z^2} - M^2(x-x_1)}{\beta^2}]\} \qquad (A.15)$$

$$Q = (x_2 - x_1)(y - y_1) - (x - x_1)(y_2 - y_1)$$

By applying the following transformation, the line integrals in equation (A.14) can be reduced to a definite integral.

$$x - \zeta = x - x_1 - \tau(x_2 - x_1)$$

$$y - \eta = y - y_1 - \tau(y_2 - y_1) \qquad (A.16)$$

Thus, the first integral in equation (A.14) becomes:

$$= \int_o^1 (\frac{1}{(y_2 - y_1)\sqrt{A\tau^2 + \beta\tau + c}} *$$

$$\{Q \frac{[(x_2-x_1)(y_2-y_1)\tau-(y-y_1)(x_2-x_1)+Q](x_2-x_1)+\beta^2(y_2-y_1)^2[(y_2-y_1)\tau-(y-y_1)]}{}\})$$

$$+ (- \frac{i\omega}{V_\infty})\{\frac{M[(y-y_1)-\tau(y_2-y_1)]}{\sqrt{A\tau^2+ \beta\tau + c}} - (\frac{M}{\beta^2} \frac{x_o}{R} - \frac{M^2}{\beta^2}) \frac{x_2-x_1}{y_2-y_1}\} *$$

$$\exp\left\{-\frac{i\omega}{V_\infty}\frac{M\sqrt{A\tau^2+B\tau+C} - M^2[x-x_1-\tau(x_2-x_1)]}{\beta}\right\} * (y_2-y_1)d\tau \tag{A.17}$$

The second integral in equation (A.14) becomes:

$$\int_o^1 \left(F\left(\frac{i\omega}{V_\infty}\frac{M[(y-y_1)-\tau(y_2y_1)]}{(A\tau^2+B\tau+C)^{3/2}}\beta^2z^2 + \frac{i\omega}{V_\infty}\frac{Mzx_o}{R^3}\left(\frac{x_2-x_1}{y_2-y_1}\right)\right) * \right.$$

$$\exp\left\{-\frac{i\omega}{V_\infty\beta^2}\left(M\sqrt{A\tau^2+B\tau+C} - M^2[(x-x_1)-\tau(x_2-x_1)]\right\}\right)(y_2-y_1)d\tau \tag{A.18}$$

The last integral in equation (A.14) is

$$= \int_o^1 \left(F * \frac{i\omega}{V_\infty}\frac{M[(y-y_1)-\tau(y_2-y_1)}{\sqrt{A\tau^2+B\tau+C}} + \frac{i\omega}{V_\infty}\left(\frac{M}{\beta^2}\frac{x_o}{R} - \frac{M^2}{\beta^2}\right)\frac{x_2-x_1}{y_2-y_1} * \right.$$

$$\exp\left\{-\frac{i\omega}{V_\infty}\frac{M\sqrt{A\tau^2+B\tau+C} - M^2[x-x_1-\tau(x_2-x_1)]}{\beta^2}\right\}\Big)(y_2-y_1)d\tau \tag{A.19}$$

where:

$$A = (x_2-x_1)^2 + \beta^2)y_2-y_1)^2 \tag{A.20a}$$

$$B = -2[(x-x_1)(x_2-x_1) + \beta^2(y-y_1)(y_2-y_1)] \tag{A.20b}$$

$$C = (x-x_1)^2 + \beta^2(y-y_1)^2 + \beta^2z^2 \tag{A.20c}$$

To evaluate these integrals, parabolic approximation of the following form is used:

$$J = \int \frac{dk}{dz}\cos\lambda_J d\ell = \int_{-e}^{e}\frac{A\eta^2 + B\eta + C}{(\eta_o-\eta)^2 + \zeta^2}d\eta \tag{A.21}$$

where:

$$A = \frac{K_l - 2K_m + K_o}{2e^2}$$

$$B = \frac{K_o - K_i}{2e}$$

$$C = K_m$$

m stands for midpoint.

Expressions from ϕ_2

Applying integration by part to ϕ_2 , the result becomes

$$\phi_2 = -\frac{i\omega}{V_\infty}\frac{\Delta C_p}{8\pi}\left[\tan^{-1}\frac{2a\tau + b}{2(y_2-y_1)z}\, I \,\Big|_L - \int_L \mathrm{Tan}^{-1}\frac{2a\tau + b}{2(y_2-y_1)z}\frac{\partial I}{\partial\eta}\, d\eta\right. \quad (A.22)$$

Differentiating ϕ_2 with respect to z gives

$$\frac{\partial\phi_2}{\partial z} = -\frac{i\omega}{V_\infty}\frac{\Delta C_p}{8\pi}\left\{-\frac{y_2-y}{(y_2-y)^2+z^2} I_2 + \frac{y_1 - y}{(y_1-y)^2 + z^2} I_1 +\right.$$

$$\mathrm{Tan}^{-1}\frac{y_2-y}{z}\frac{\partial I_2}{\partial z} - \mathrm{Tan}^{-1}\frac{y_1-y}{z}\frac{\partial I_1}{\partial z} + \int_L \left[\frac{2(2a\tau+b)(y_2-y_1)}{4(y_2-y_1)^2 z^2+(2a\tau+b)^2}\frac{\partial I}{\partial\eta} -\right.$$

$$\left.\mathrm{Tan}^{-1}\frac{2a\tau+b}{2(y_2-y_1)z}\frac{\partial^2 I}{\partial z\partial\eta}\right]d\eta\Big\} \quad (A.23)$$

where:

$$a = (y_2 - y_1)^2$$

$$b = -2(y - y_1)(y_2 - y_1)$$

$$c = (y - y_1)^2 + z^2$$

$$I_2 = \int_{(\tau_1 r_1)_1}^{\infty} \left(1 - \frac{\tau'}{\sqrt{\tau'^2 + r_{12}^2}}\right) e^{-\frac{i\omega}{V_\infty}(\tau' + x_{02})} d\tau' \tag{A.24}$$

$$I_1 = \int_{(\tau_1 r_1)_1}^{\infty} \left(1 - \frac{\tau'}{\sqrt{\tau'^2 + r_{11}^2}}\right) e^{-\frac{i\omega}{V_\infty}(\tau' + x_{01})} d\tau' \tag{A.54}$$

$$I = \int_{(\tau_1 r_1)}^{\infty} \left(1 - \frac{\tau'}{\sqrt{\tau'^2 + r_1^2}}\right) e^{-\frac{i\omega}{V_\infty}(\tau' + x_0)} d\tau' \tag{A.26}$$

$$(\tau_1 r_1)_2 = \frac{-(x-x_2) + M\sqrt{(x-x_2)^2 + \beta^2 (y-y_2)^2 + \beta^2 z^2}}{\beta^2}$$

$$(r_{12})^2 = (y - y_2)^2 + z^2$$

$$x_{02} = (x - x_2) - \tau(x_2 - x_1)$$

$$(r_{11})^2 = (y - y_1)^2 + z^2$$

$$(\tau_1 r_1)_1 = \frac{-(x-x_1) + M\sqrt{(x-x_1)^2 + \beta^2 (y-y_1)^2 + \beta^2 z^2}}{\beta^2}$$

$$x_{01} = (x - x_1) - \tau(x_2 - x_1)$$

Differentiating I, I_1, I_2 with respect to z and η gives

$$\frac{\partial I}{\partial z} = -\frac{Mz}{R}\left(1 - \frac{\tau_1}{\sqrt{1+\tau_1^2}}\right) e^{-\frac{i\omega}{V_\infty}(\tau_1 r_1 + x_0)} + z\int_{\tau_1 r_1}^{\infty} \frac{\tau'}{(\tau'^2 + r_1^2)^{3/2}} e^{-\frac{i\omega}{V_\infty}(\tau' + x_o)} d\tau' \tag{A.27}$$

$$\frac{\partial I_1}{\partial z} = -\frac{Mz}{R_1}\left(1 - \frac{\tau_{11}}{\sqrt{1+\tau_{11}^2}}\right) e^{-\frac{i\omega}{V_\infty}[(\tau_1 r_1)_1 + x_{01}]} + z\int_{(\tau_1 r_1)_1}^{\infty} \frac{\tau'}{(\tau'^2 + r_{11}^2)^{3/2}} e^{-\frac{i\omega}{V_\infty}(\tau' + x_{01})} d\tau' \tag{A.28}$$

$$\frac{\partial I_2}{\partial z} = - \frac{Mz}{R_2} \left(1 - \frac{\tau_{12}}{\sqrt{1+\tau_{12}^2}}\right) e^{-\frac{i\omega}{V_\infty}[(\tau_1 r_1)_2 + x_{02}]} +$$

$$z \int_{(\tau_1 r_1)_2}^{\infty} \frac{\tau'}{(\tau'^2 + r_{12}^2)^{3/2}} e^{-\frac{i\omega}{V_\infty}(\tau' + x_{02})} d\tau' \qquad (A.29)$$

$$\frac{\partial I}{\partial \eta} = \frac{M(y-n)}{R} \left(1 - \frac{\tau_1}{\sqrt{1+\tau_1^2}}\right) e^{-\frac{i\omega}{V_\infty}(\tau_1 r_1 + x_0)} - (y-\eta) \int_{\tau_1 r_1}^{\infty} \frac{\tau' e^{-\frac{i\omega}{V}(\tau' + x_0)}}{(\tau'^2 + r_1^2)^{3/2}} d\tau$$

$$+ \frac{i\omega}{V_\infty} I\left(\frac{x_2 - x_1}{y_2 - y_1}\right) + \left(1 - \frac{\tau_1}{\sqrt{1+\tau_1^2}}\right) e^{-\frac{i\omega}{V_\infty}(\tau_1 r_1 + x_0)} \left(\frac{Mx_0}{\beta^2 R} - \frac{1}{\beta^2}\right) \frac{x_2 - x_1}{y_2 - y_1} \qquad (A.30)$$

$$\frac{\partial^2 I}{\partial z \partial \eta} = \frac{z}{r_1} \{ e^{-\frac{i\omega}{V_\infty}(\tau_1 r_1 + x_0)} \frac{M(y-\eta)}{R} \left[- \frac{r_1 \beta^2}{R^2} \left(1 - \frac{\tau_1}{\sqrt{1+\tau_1^2}}\right) - \right.$$

$$\left. \frac{1}{(1+\tau_1^2)^{3/2}} \left(\frac{M}{R} - \frac{\tau_1}{r_1}\right) + \frac{1}{r_1} \frac{\tau_1}{(1+\tau_1^2)^{3/2}} \right] -$$

$$\frac{i\omega}{V_\infty} \left[\frac{M^2 (y-\eta)}{R^2}\right] r_1 \left(1 - \frac{\tau_1}{\sqrt{1 + \tau_1^2}}\right) e^{-\frac{i\omega}{V_\infty}(\tau_1 r_1 + x_o)} +$$

$$\frac{i\omega}{V_\infty} \frac{\partial I}{\partial r_1} \frac{x_2 - x_1}{y_2 - y_1} - \frac{1}{(1+\tau_1^2)^{3/2}} e^{-\frac{i\omega}{V_\infty}(\tau_1 r_1 + x_0)} \left(\frac{Mx_0}{\beta^2 R} - \frac{1}{\beta^2}\right) \frac{x_2 - x_1}{y_2 - y_1} \left(\frac{M}{R} - \frac{MR - x_0}{\beta^2 r_1^2}\right) -$$

$$- \frac{i\omega}{V_\infty} \left(1 - \frac{\tau_1}{\sqrt{1+\tau_1^2}}\right) e^{-\frac{i\omega}{V_\infty}(\tau_1 r_1 + x_0)} \left(\frac{Mx_0}{\beta^2 R} - \frac{1}{\beta^2}\right) \frac{x_2 - x_1}{y_2 - y_1} \frac{Mr_1}{R} +$$

$$\left(1 - \frac{\tau_1}{\sqrt{1+\tau_1^2}}\right) e^{-\frac{i\omega}{V_\infty}(\tau_1 r_1 + x_0)} \left(-\frac{M x_0 r_1}{R^3}\right) \frac{x_2 - x_1}{y_2 - y_1}\} +$$

$$\frac{3(y-\eta)z}{r_1^2} [r_1^2 \int_{T_1 r_1}^{\infty} \frac{\tau' e^{-\frac{i\omega}{V_\infty}(\tau'+x_0)}}{(\tau'^2+r_1^2)^{5/2}} d\tau'] \tag{A.31}$$

$$\frac{dI}{dr_1} = \left(1 - \frac{\tau_1 r_1}{\sqrt{\tau_1^2 r_1^2 + r_1^2}}\right) e^{-\frac{i\omega}{V_\infty}(\tau_1 r_1 + x_0)} \left(-\frac{M r_1}{R}\right) +$$

$$\int_{\tau_1 r_1}^{\infty} \frac{\tau_1 r_1}{(\tau'^2+r_1^2)^{3/2}} e^{-\frac{i\omega}{V_\infty}(\tau'+x_0)} d\tau' \tag{A.32}$$

To evaluate the integrals in the $\frac{\partial \phi_2}{\partial z}$ term, the following approximation may be used in I, I_1, and I_2 terms (ref. 15):

$$\frac{\tau}{\sqrt{1+\tau^2}} \approx 1 - \sum a_n e^{-c_n \tau} \tag{A.33}$$

n	c_n	a_n
1	0.0625	0.002907843
2	0.125	0.002591528
3	0.25	0.02667074
4	0.5	0.07097100
5	1	0.3478370
6	2	0.5556069
7	3	0.7048426
8	4	-0.7769790
9	8	0.07004561
10	16	-0.004557519

Therefore, by applying the above approximation (eq. A.33), I, I_1, I_2 can be integrated exactly. Note that integrals in the form of

$$J = \int \frac{ue^{iku}}{(1+u^2)^{3/2}}\,du \quad , \quad P = \int \frac{ue^{iku}}{(1+u^2)^{5/2}}\,du \qquad (A.34)$$

can be reduced into form like I by taking integration by parts. For P, twice integration by part is necessary.

By the same approach, the u and v velocity can be obtained.

To check the expressions, it should be noted that the induced downwash due to an oscillating line vortex can be reduced to the downwash velocity due to a steady line vortex if the oscillating frequency (ω) is set to zero. In this case, equation (A.14) becomes

$$\frac{d\phi}{dz}\Big|_{\omega=0} = \frac{\Delta C_p}{8\pi}\,\frac{dF}{dz}\Big|_L \qquad (A.35)$$

where:

$$F = \int_L \left(\frac{x_0}{Rr_1^2}\right) z_0\,d\eta + \mathrm{Tan}^{-1}\left[\frac{z(x_1-x)}{(y_1-y)\sqrt{(x_1x)^2+\beta^2(y_1y)^2+\beta^2z^2}}\right]$$

$$- \mathrm{Tan}^{-1}\left[\frac{z(x_2-x)}{(y_2-y)\sqrt{(x_2-x)^2+\beta^2(y_2-y)^2+\beta^2z^2}}\right] \qquad (A.36)$$

and

$$\frac{dK}{dz}\Big|_L = \frac{1}{\sqrt{(x-x_2)^2+\beta^2(y-y_2)^2+\beta^2(z-z_2)^2}} \,*$$

$$\left\{Q\,\frac{(x_2-x_1)(x_2-x)+\beta^2(y_2-y_1)(y_2-y)+\beta^2(z_2-z)(z_2-z_1)}{Q^2+(z-z_2)2[(x_2-x_1)^2+\beta(y_2-y_1)^2]}\right\}$$

$$- \frac{1}{\sqrt{(x-x_1)^2+\beta^2(y-y_1)^2+\beta^2(z-z_1)^2}} *$$

$$\{Q \frac{(x_2-x_1)(x_1-x)+\beta^2(y_2-y_1)(y_1-y)+\beta^2(z_1-z)(z_2-z)}{Q^2+(z-z_1)^2[(x_2-x_1)^2+\beta^2(y_2-y_1)^2]}\} \qquad (A.37)$$

Equation (A.37) exactly matches the downwash velocity due to a steady line vortex.

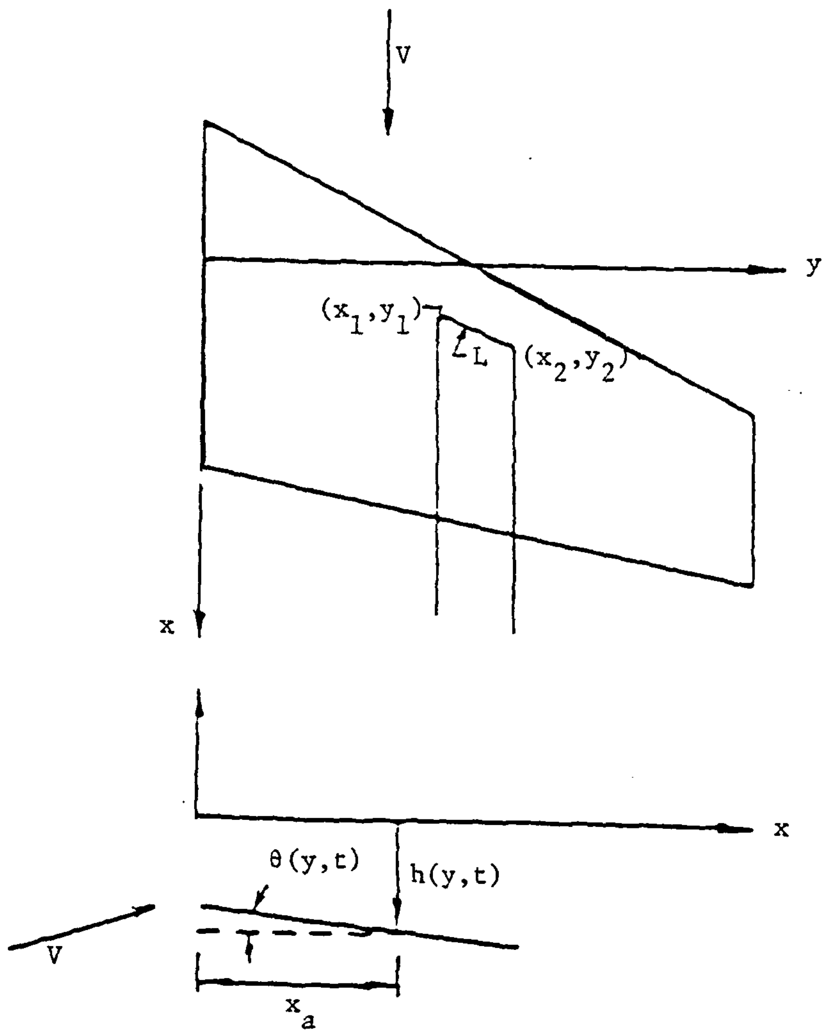

Figure A.1 Definition of Geometry in Oscillatory Motions